

Branch points of homotopies: Distribution and probability of failure

Jonathan D. Hauenstein^{1*} Caroline Hills^{1†} Andrew J. Sommese¹
Charles W. Wampler^{1‡}

¹Department of Applied and Computational Mathematics and Statistics,
University of Notre Dame, Notre Dame, IN 46556
{hauenstein, chill1, sommese, cwampler}@nd.edu

Abstract

Homotopy continuation is a standard method used in numerical algebraic geometry for solving multivariate systems of polynomial equations. Techniques such as the so-called gamma trick yield trackable homotopies with probability one. However, since numerical algebraic geometry employs numerical path tracking methods, being close to a branch point may cause concern with finite precision computations. This paper provides a systematic study of branch points of homotopies to elucidate how branch points are distributed and use this information to study the probability of failure when using finite precision. Several examples, including a system arising in kinematics, with various start systems are included to demonstrate the theoretical analysis.

Keywords: homotopy continuation, branch points, ramification points, path tracking, probability of failure, numerical algebraic geometry

1 Introduction

Homotopy continuation is a method that has been used to solve many problems in mathematics, science, and engineering. By starting with a known solution set to a given system of equations $g = 0$, one can use homotopy continuation to deform from system g to a target system f to find the solutions of $f = 0$ [1, 22]. In this paper, we consider multivariate polynomial systems over the complex numbers, in which case g can be chosen to guarantee, with probability one, that all isolated solutions of f will be found by tracking solution paths starting at the solutions of $g = 0$. The techniques of numerical algebraic geometry generalize this functionality to find all solution sets regardless of their dimension [32]. To be more precise, success with “probability one” means that certain parameters can be chosen generically in a nonempty Zariski-open set in which the solution paths exist and are nonsingular. The working assumption in practice is that making the choice of these parameters using a pseudo-random number generator is equivalent to choosing them generically. While this is a well-justified assumption, the fact remains that these paths must be tracked numerically and may pass near branch point singularities. Hence, the number of branch points and their distribution impact the probability of failure in a numerical implementation.

*Supported in part by NSF CCF-2331400, Simons Foundation SFM-00005696, and the Robert and Sara Lumpkins Collegiate Professorship.

†Supported in part by NSF CCF-2331400 and the Robert and Sara Lumpkins Collegiate Professorship.

‡Supported in part by the Huisking Foundation, Inc. Collegiate Research Professorship.

Let U be \mathbb{C}^N or a compactification thereof, such as a product of projective spaces. Our objective is to numerically solve the polynomial system $f(u) : U \rightarrow \mathbb{C}^N$ starting from a polynomial system $g(u) : U \rightarrow \mathbb{C}^N$ and its isolated solutions by tracking the solution paths of the homotopy

$$h(u, t) = \gamma t g(u) + (1 - t) f(u), \quad t \in (0, 1] \subset \mathbb{R} \quad (1)$$

where $\gamma = e^{i\theta}$ in which the angle θ is chosen uniformly on $[-\pi, \pi]$ and $i = \sqrt{-1}$. When U is a product of projective spaces, u is a set of homogeneous coordinates and one may choose to work on a randomly selected coordinate patch [20] or adaptively switch patches as a path is tracked [16]. Our convention is to start at $t = 1$ and end at $t = 0$, which is convenient in cases where a singular endgame is invoked as $t \rightarrow 0$. As we will be studying in detail, the inclusion of the random number γ , sometimes called the “gamma trick,” allows the homotopy path to avoid branch point singularities with probability one. For each $t \in \mathbb{C}$, define $V(h(\cdot, t)) := \{u \in U \mid h(u, t) = 0\}$. To be more precise, for a properly defined homotopy, there are a finite number of $t \in \mathbb{C}$ where the Jacobian matrix $\frac{\partial h}{\partial u}(u, t)$ loses rank for some $u \in V(h(\cdot, t))$. By choosing θ at random, one in effect moves these branch points so that the probability of the corresponding ramification points lying on $(0, 1]$ becomes zero. Nevertheless, there is no guarantee about how close to this segment some may fall. If one is too close to this segment, the ill-conditioning of the Jacobian in its neighborhood may cause a path tracker implemented in finite-precision floating point arithmetic to fail. The focus of this article is to examine how the branch points of several classes of polynomial systems are distributed and use this information to study how the probability of failure behaves in finite precision.

Equation (1) implicitly defines solution paths. One approach to computing them numerically is to choose a coordinate patch on U , say $u = u(q)$, for $q \in \mathbb{C}^N$, and then differentiate (1) with respect to t to obtain the Davidenko differential equation:

$$h_u \cdot \frac{\partial u}{\partial q} \cdot \frac{dq}{dt} + h_t = 0, \quad \text{where} \quad h_u = \frac{\partial h}{\partial u} \quad \text{and} \quad h_t = \frac{\partial h}{\partial t}. \quad (2)$$

For example, if u is a set of $N + 1$ homogeneous coordinates on \mathbb{P}^N , one may choose a patch $u = Aq$ where $A \in \mathbb{C}^{(N+1) \times N}$ is a full-rank matrix satisfying $\text{rank}(h_u A) = \text{rank}(h_u)$. This will be true for a nonempty Zariski-open subset of $\mathbb{C}^{(N+1) \times N}$, so a random choice will suffice with probability one [20]. However, one may improve numerical conditioning by adaptively switching patches as a path is tracked [16]. Similar constructions work when U is a product of projective spaces with an adjustment in the number of rows in A .

Starting from any initial solution u_0 such that $h(u_0, 1) = \gamma g(u_0) = 0$, standard numerical methods for solving differential equations allow one to move monotonically in t from 1 towards 0 along paths that are uniquely defined as long as h_u is nonsingular. For example, on the patch $u = Aq$, one may use a forward Euler predictor with step size $\Delta t < 0$, namely

$$u_{j+1} = u_j - [h_u(u_j, t_j)A]^{-1} h_t(u_j, t_j) \Delta t, \quad t_{j+1} = t_j + \Delta t$$

to move along t and, after incrementing $j \leftarrow j + 1$, correct the prediction using one or more iterations of Newton’s method,

$$u_j \leftarrow u_j - [h_u(u_j, t_j)A]^{-1} h(u_j, t_j)$$

to move (u_j, t_j) closer to the exact solution path. Although higher-order prediction methods are utilized in practice, such as Runge-Kutta methods [4] and Padé approximations [33], this does not change the gist of the discussion here. If the prediction is close enough and $h_u A$ is well-conditioned, the correction steps converge quadratically to the exact path. However, when h_u is ill-conditioned, the accuracy of the prediction decreases and may step outside the convergence zone for Newton’s

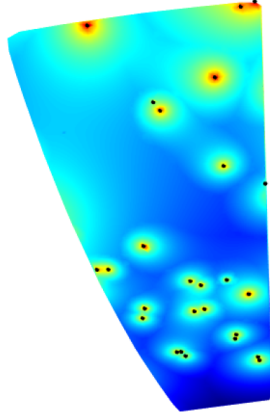


Figure 1: Illustrating on a small region the logarithm of the maximum condition number for each solution in relationship to the location of the ramification points (black). Proximity to ramification points increases the maximum condition number in the surrounding space resulting in “hot spots.”

method. Even if the prediction is in the theoretical convergence zone, convergence of Newton’s method may be lost if the digits of precision used are not enough to overcome ill-conditioning.

Failure near a branch point can happen in several ways, depending in part on how path tracking is implemented. One common failure mode is path crossing, due to the fact that branch points arise where solution paths cross. As t passes near a branch point, it may happen that the prediction lands within the convergence zone of another nearby path, ultimately causing the algorithm to omit from its list of solutions the endpoint of the original path. Alternatively, an implementation may include safeguards to prevent path crossing by adaptively taking smaller step sizes when it detects that the Jacobian is near-singular and halting if progress becomes too slow. Finally, as already mentioned, convergence of the corrector requires that enough digits of precision are used. In principal, as long as γ has been chosen such that there are no branch points for $t \in (0, 1]$, some combination of small enough step size in t with large enough precision will advance the path tracker past any close encounters with branch points and allow the path tracker to complete successfully. Failure occurs if this requires more resource in time or precision than have been allocated.

An early experience motivating our interest in these matters was solving the nine-point path synthesis problem in [38]. Over thirty years ago, suspicious paths were recomputed in quadruple precision and symmetry checks were employed to assure a complete solution list. After the development of a path tracker with adaptive precision [6], the problem was revisited in [7] where it was found that 0.83% of paths required more than double precision for reliable tracking. The formulation used consists of 4 quadric and 8 quartic polynomials with a 2-homogeneous Bézout number (root count) of 286,720, which is the number of paths in the homotopy. Experience with many such systems shows that higher degrees and larger Bézout numbers tend to require higher precision, which leads us presently to investigate more deeply how these are related. Figure 1 illustrates the relationship between the condition number and presence of branch points. As suggested by this image, the need for higher precision based on ill-conditioning is associated with the presence of branch points. Therefore, we investigate here the number and distribution of branch points.

Previous work has addressed the influence of branch points on the path through adaptive strategies to improve efforts in homotopy step-size and precision [6, 33, 34], scaling coefficients with the SCLGEN algorithm [21], and Jacobian scaling [13, 16]. Certified path tracking methods take adaptivity a step further, using either alpha-theory or techniques from interval arithmetic to

guarantee that the numerical approximations never leave the zone of convergence of the original path [10, 15, 19]. Some examples of results related to condition numbers, probability of success, and complexity analysis for homotopy continuation are provided in [2, 11, 12, 25–30]. Although these aforementioned methods do not change the actual path tracked, monodromy techniques can be used to alter a homotopy path to circle around branch points before resuming along the original path [8]. These methods provide a local look at the branch points near a given homotopy path, which are generally effective in practice. Nonetheless, they do not consider the location of branch points with regards to all possible homotopy paths.

For a single run of a homotopy, only the branch points close to the homotopy path matter. The novel aspect of this article is a global view of branch points. In particular, this article considers the distribution of all the branch points and studies how this impacts the probability of success or failure in tracking all the paths of the homotopy.

The rest of the paper is organized as follows. Section 2 presents the mathematical formulations for defining a homotopy in projective space, mapping to the Riemann sphere, and visualization. Section 3 discusses how to compute branch points. Section 4 evaluates the distance from a branch point to a homotopy path and proposes a model of path tracking failure and endgame failure based on the closest corresponding ramification point. Section 5 provides examples of these analyses for quadratic systems in various number of variables and a four-bar path synthesis system. Finally, Section 6 summarizes our findings and presents an interesting question for further study.

2 Pencils, branch points, and sphere mappings

To aid in analysis and visualization, we reformulate homotopy (1) on projective space and apply a Riemann sphere mapping.

2.1 Projective space and pencils

While (1) is an appropriate formulation for running a single instance of a homotopy with $t \in (0, 1]$, to study the full set of possible homotopies for all possible choices of γ , it is more appropriate to recast the homotopy using projective space as

$$h(u, \tau) = h(u, [a, b]) = ag(u) + bf(u), \quad \tau = [a, b] \in \mathbb{P}^1. \quad (3)$$

When f and g are polynomial systems of the same class, h is said to be a *pencil* of that class.

Example 1 (N general quadrics with Bézout start system). To solve a system of N general quadrics in \mathbb{P}^N , one standard homotopy begins with start system g whose roots are roots of unity:

$$g(u) = \{g_1(u), \dots, g_N(u)\}, \quad g_j(u) = u_j^2 - u_0^2.$$

Let the target system $f(u)$ be a system of N general, complex quadrics in $N + 1$ variables. That is, $f(u) = \{f_1(u), \dots, f_N(u)\}$ where

$$f_i(u) = \underline{u}A_i\underline{u}^T, \quad \underline{u} = [u_0 \quad u_1 \quad \cdots \quad u_N] \in \mathbb{P}^N,$$

where each $A_i \in \mathbb{C}^{(N+1) \times (N+1)}$ is symmetric with general complex elements. For random instances, we choose each element in A_i uniformly within the box $[-1, 1] \times [-i, i] \subset \mathbb{C}$. Hence, with probability one, there are 2^N solutions in \mathbb{P}^N to both $g(u) = 0$ and $f(u) = 0$. The case with $N = 6$ will be the running example throughout.

2.2 Branch points

Let $\pi_\tau(u, \tau) = \tau$ be the natural projection of $U \times \mathbb{P}^1$ onto \mathbb{P}^1 . We assume that among the components of the algebraic set $V(h) := \{(u, \tau) \in U \times \mathbb{P}^1 \mid h(u, \tau) = 0\}$, there is a curve $X \subset U \times \mathbb{P}^1$ whose generic points have full rank, i.e., $\text{rank } h_u = N$, which implies that $\pi_\tau(X)$ is a D -sheeted cover of \mathbb{P}^1 for some $D \in \mathbb{Z}_{>0}$. This is the usual setup when h is a homotopy for solving system f by tracking D solution paths as $\tau \rightarrow [0, 1] \in \mathbb{P}^1$ along a continuous 1-dimensional real path $\gamma(t) \in \mathbb{P}^1$, $t \in [0, 1] \subset \mathbb{R}$. We call $\gamma(t)$ the *homotopy path* and $X \cap \pi_\tau^{-1}(\gamma(t))$ the set of D *solution paths*. Throughout this article, we assume that $\gamma(1) = [1, 0]$ and $\gamma(0) = [0, 1]$.

Let Z be the points in X where h_u drops rank. By our assumption regarding the generic nonsingularity of X , Z is a finite set. We may partition Z into three distinct subsets as

$$Z = Z_0 \sqcup Z_1 \sqcup Z_B, \quad \text{such that} \quad \pi_\tau(Z_0) = [0, 1], \quad \pi_\tau(Z_1) = [1, 0], \quad Z_B = Z \setminus (Z_0 \cup Z_1). \quad (4)$$

Accordingly, Z_0 is the singular set of $X \cap V(f)$, Z_1 is the singular set of $X \cap V(g)$, and Z_B are the *branch points* of X . Moreover, $B = \pi_\tau(Z_B)$ are the *ramification points* of X with respect to τ . In many cases, where h is a homotopy for solving f *ab initio* [9], g is a start system constructed to have no singularities, in which case $Z_1 = \emptyset$. For all homotopies considered here, the map $\pi_\tau : Z_B \rightarrow B$ is one-to-one, i.e., there is a unique branch point corresponding to each ramification point. The relationship between branch points and ramification points is studied in general in [31]. Due to the one-to-one relationship and ease of viewing, we will plot ramification points. For example, Figure 1 illustrates ramification points on a region in \mathbb{P}^1 as a proxy for branch points.

If the homotopy path passes through a ramification point, there are solution paths where the Davidenko differential equation (2) fails to define a unique solution path through the corresponding branch point. The singularities Z_0 and Z_1 present a different numerical problem since these correspond with endpoints and startpoints, respectively, of the solution paths. Since the value of τ is known *a priori* there, one may treat these using a local analysis based on the existence of a Puiseux series. A case where $Z_1 \neq \emptyset$ arises in polyhedral (a.k.a. BKK) homotopies [17, 36] where an analysis of the Newton polytopes of g provides the initial terms of the Puiseux series enabling the method to step off of $t = 1$. When $Z_0 \neq \emptyset$, that is, when f has singular solutions, endgame methods sample the solution paths in the vicinity of $t = 0$ to compute the endpoint value without needing to track all the way to the origin. These methods may approximate the initial terms of the Puiseux series directly [17, 24] or use the Cauchy integral theorem [23]. We will discuss endgames further in Section 4.3.

2.3 Riemann sphere

To help visualization, it is convenient to map $\tau = [a, b] \in \mathbb{P}^1$ to the Riemann sphere $(x, y, z) \in \mathbb{S}^2$, i.e., the unit sphere in \mathbb{R}^3 , using the following two charts:

$$b \neq 0 : \quad w = a/b, \quad (x, y, z) = (2\Re(w), \quad 2\Im(w), 1 - ww^*)/(1 + ww^*), \quad (5)$$

$$a \neq 0 : \quad w = b/a, \quad (x, y, z) = (2\Re(w), -2\Im(w), ww^* - 1)/(1 + ww^*), \quad (6)$$

where $\Re(w)$ and $\Im(w)$ are the real and imaginary parts of w , respectively. One may confirm that these charts agree where they are both valid. Charts for mapping in the inverse direction are

$$z \neq -1 : \quad [a, b] = [x + iy, z + 1], \quad (7)$$

$$z \neq 1 : \quad [a, b] = [1 - z, x - iy]. \quad (8)$$

These maps are bijective, so we may speak of a path in \mathbb{P}^1 and its image on the Riemann sphere as the same path, letting context determine which is applicable.

Substituting $[a, b] = [e^{i\theta}t, 1 - t]$ into both (5) and (6), one finds that the homotopy (1) follows a meridian—a great circle arc of constant longitude θ on the Riemann sphere—starting at $(0, 0, -1)$ corresponding with $t = 1$ and $\tau = [1, 0]$, and ending at $(0, 0, 1)$ corresponding with $t = 0$ and $\tau = [0, 1]$. We will refer to this great semicircle as the *homotopy path of longitude θ* .

The upshot of this reformulation of the problem is that the branch points of homotopy (3) are fixed and so are the ramification points in \mathbb{P}^1 and thereby on the Riemann sphere. Choosing θ at random picks the longitude of the arc that is tracked in executing the homotopy. Arcs that pass through a ramification point will result in a path-tracking failure, and in practical implementation, failures may also occur for near misses. Hence, the distribution of branch points, ramification points, and their distances to arcs of constant longitude become of vital interest.

In what follows, we will also refer to the latitude of branch points on the Riemann sphere. Measuring the angle in radians from $(x, y, z) = (0, 0, 1)$, the latitude is $\phi = \cos^{-1} z$.

2.4 Visualization of branch points

In Section 3 below, we will discuss how we compute branch points, but for the moment assume we already know them and we wish to visualize their distribution via the corresponding ramification points. For this purpose, we will use scatter plots, heat maps, and histograms. The first step is to use (5) and (6) to map the ramification points to the unit sphere. Any single 2D image of this sphere shows only the forward facing hemisphere and has the drawback of exaggerating the apparent density of points near the boundary of that hemisphere. To overcome this, we make scatter plots of the points using polar coordinates using the following:

$$(r, \theta) = \begin{cases} (\sqrt{1+z}, \arctan2(y, x)), & z < 0, \\ (\sqrt{1-z}, \arctan2(-y, -x)), & z \geq 0, \end{cases} \quad (9)$$

where $\arctan2$ is the two-argument arctangent function. These maps produce two circular disks, one for each hemisphere divided by the equator, $z = 0$. We will present these by placing the map for $z \geq 0$ to the right and tangent to the one for $z < 0$, touching at the image of $(x, y, z) = (1, 0, 0)$. In this two-disk image, the great circle defined by $y = 0$, which represents real $[a, b]$, is a horizontal line segment. Its midpoint is the image of $(x, y, z) = (1, 0, 0)$ and both endpoints correspond to $(x, y, z) = (-1, 0, 0)$. The center of the left-hand disk corresponds to the start system g (i.e., $[a, b] = [1, 0]$) and the center of the right-hand disk corresponds to f (i.e., $[a, b] = [0, 1]$). Due to the area-preserving property of this map, even though distances are distorted near the perimeters of the disks, a uniform density of points on the sphere will produce a uniform density of points in these disks. Figure 2 shows the result for the homotopy constructed using $N = 6$ in Example 1, which has 1344 branch points and ramification points. Also shown in that figure is a heat map of ramification point density, wherein each pixel is colored according to how many ramification points are within a specified distance on the unit sphere. (In this paper, a distance of 0.08 rad is used throughout.) For larger N , where the number of branch points becomes large, a scatter plot of ramification points becomes too crowded and only the heat map is informative.

A third way to visualize the distribution of branch points is to plot histograms of longitude and z -coordinate of the ramification points. Dividing longitude into equal sectors divides the sphere into equal areas and the same is true for equal increments of the z -coordinate. Consequently, if the ramification points are uniformly distributed on the sphere, both these histograms will be flat within statistical variation. Figure 3 suggests uniformity with respect to longitude but not with respect to the z -coordinate for the running example.

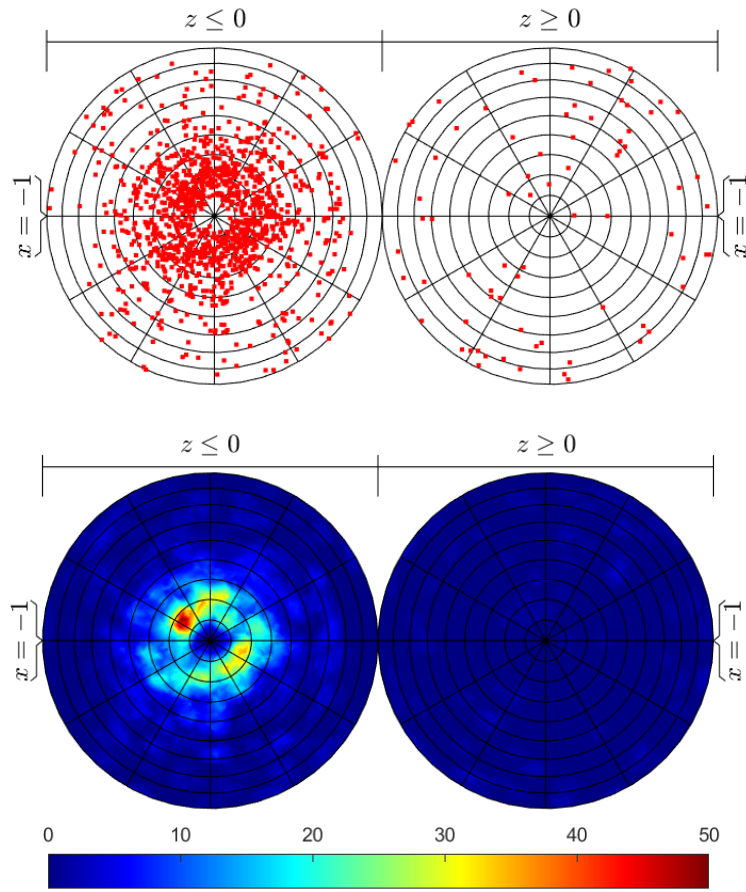


Figure 2: Ramification point scatter plot and heat map for $N = 6$ in Example 1.

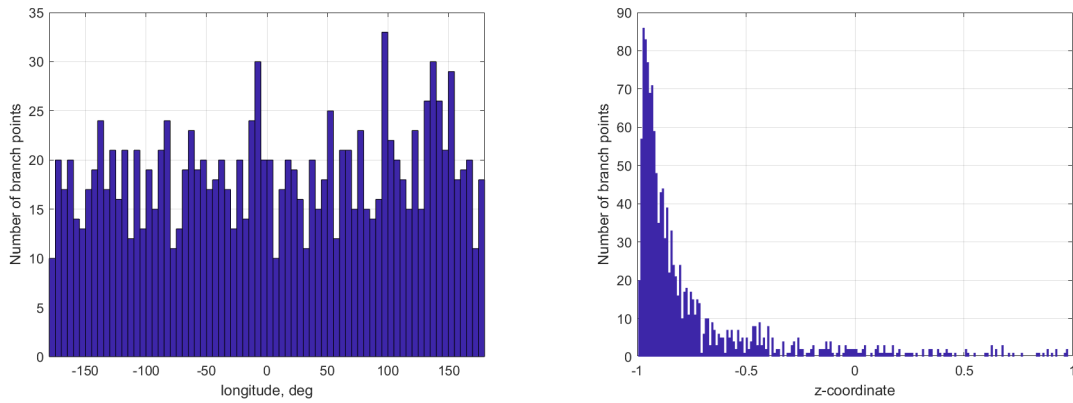


Figure 3: Histograms of longitude and z -coordinate for $N = 6$ in Example 1.

We note that in this particular example, the ramification points are concentrated in a ring between 10° to 20° centered on $(0, 0, -1)$, which corresponds with the start system. Examples in Section 5 show a similar characteristic of the Bézout start system with a complete absence of branch points in a disk centered there, and an overconcentration of branch points just outside that disk.

3 Computing branch points

In order to employ the visualization techniques described in Section 2.4, one needs a method to compute the branch points. We begin by computing the set $Z = X \cap V(\text{rank } h_u < N)$, and then we partition this into Z_0, Z_1, Z_B as in (4), with ramification points $B = \pi_\tau(Z_B)$. If $V(h)$ has solution components other than X , an intersection algorithm would be required to compute Z , but for the examples considered in this paper, the start system g is general enough that the only possible components of $V(h)$ other than X are singular components of the end point system, $h(u, 0) = f$. As for the right-hand element of the intersection, formulating algebraic conditions for the drop in rank of h_u in terms of determinants is inconvenient, particularly due to the possibly high degree. Instead, we may express the loss of rank condition as the existence of a null-space vector [3] either on the left or right. With these facts in mind, we can find the branch points by computing all isolated solutions of either

$$B_\ell(u, \tau, v) = \{h(u, \tau), v h_u(u, \tau)\} : U \times \mathbb{P}^1 \times \mathbb{P}^{N-1} \quad (10)$$

where v is a $1 \times N$ row of homogeneous coordinates, or as

$$B_r(u, \tau, v) = \left\{ h(u, \tau), \begin{bmatrix} h_u(u, \tau) \\ R \end{bmatrix} v \right\} : U \times \mathbb{P}^1 \times \mathbb{P}^{K-1} \quad (11)$$

where v is a column of K homogeneous coordinates, the number of which depends on how the compactification of U has been formulated. Matrix R is selected generically with the dimensions required to complete a square $K \times K$ matrix. If h_u is rank deficient, then so is this square matrix. Since the formulation of X ensures that there are a finite number of branch points, the right-null condition will intersect X transversely at these with probability one. However, the right-null condition allows extraneous roots where the rows of h_u are independent but R does not complete a full basis. For this reason, the right-null formulation requires a final filter that retains only the points where $\text{rank}(h_u) < N$, as can be checked numerically with a singular value decomposition. While the left-null formulation is more direct for computations, the right-null formulation is useful for proving Theorems 2 and 4 below. In the particular case when $U = \mathbb{P}^N$ so u is a set of $K = N + 1$ homogeneous coordinates on \mathbb{P}^N , R is a generic $1 \times (N + 1)$ matrix and v lives on \mathbb{P}^N . When $U = \mathbb{P}^{N_1} \times \mathbb{P}^{N_2}$, u is a set of $K = N_1 + N_2 + 2$ coordinates, and it is sufficient to choose R generically of the form

$$R = \begin{bmatrix} R_1 & 0 \dots 0 \\ 0 \dots 0 & R_2 \end{bmatrix}$$

where R_k is a $1 \times (N_k + 1)$ row vector for $k = 1, 2$.

For each of the systems we treat below, we compute branch points using the **Bertini** software package [5, 9]. Since these computations themselves are numerical homotopies, path failures and path crossings are possible, which could mean that the resulting solution lists are incomplete. However, for the general complex pencils of Example 1, our computations yield exactly the number of branch points predicted by the following.

Theorem 2. *If h is a general pencil of N polynomials of degree $d \geq 2$ in \mathbb{P}^N , then there are at most $2\binom{N+1}{2}(d-1)d^{N-1}$ branch points. In particular, when $d = 2$, the number of solution paths for h is 2^N while the number of branch points is at most $\binom{N+1}{2}2^N$.*

Proof. First, the 3-homogeneous Bézout count for system B_r in (11) is the coefficient of $\alpha^N \beta \zeta^N$ in

$$(d\alpha + \beta)^N ((d-1)\alpha + \beta + \zeta)^N \zeta$$

which is $Nd^{N-1}((N+1)(d-1)+1)$. Of course, this also yields an upper bound on the number of branch points which would be sharp if B_r was generic with respect to the 3-homogeneous structure. However, B_r is structured and this bound accounts for both branch points as well as solutions resulting from Euler's homogeneous function theorem with $u = v$, i.e., $h(u, \tau) = 0$ implies $h_u(u, \tau)u = 0$. The 2-homogeneous Bézout count for $\{h(u, \tau), Ru\}$, which is the coefficient of $\alpha^N \beta$ in $(d\alpha + \beta)^N \alpha$, is Nd^{N-1} . Due to genericity of h and R , this bound is sharp. Hence, the number of branch points is at most the difference of these two numbers, namely

$$Nd^{N-1}((N+1)(d-1)+1) - Nd^{N-1} = N(N+1)(d-1)d^{N-1} = 2\binom{N+1}{2}(d-1)d^{N-1}.$$

Moreover, when $d = 2$, this becomes $2\binom{N+1}{2}(2-1)2^{N-1} = \binom{N+1}{2}2^N$. \square

Example 3. Section 2.4 considered $N = 6$ with $d = 2$ having 1344 branch points with Figure 2 showing the 1344 ramification points. In this case, the bound from Theorem 2 is $\binom{6+1}{2}2^6 = 1344$.

Theorem 4. *If h is a general pencil of $N_1 + N_2$ polynomials of bidegree (d_1, d_2) in $\mathbb{P}^{N_1} \times \mathbb{P}^{N_2}$, then there are at most $2d_1^{N_1-1}d_2^{N_2-1}\binom{N_1+N_2}{N_1}\left(\binom{N_1+N_2+1}{2}d_1d_2 - \binom{N_2+1}{2}d_1 - \binom{N_1+1}{2}d_2\right)$ branch points. In particular, when $d_1 = d_2 = 1$ and $N = N_1 = N_2$, the number of solution paths for h is $\binom{2N}{N}$ on $\mathbb{P}^N \times \mathbb{P}^N$ while the number of branch points is at most $2N^2\binom{2N}{N}$.*

Proof. This could be seen as a special case of [31, § 3.1.2] where all polynomials in a multiprojective space have the same multidegree. On the other hand, this can be proved similarly to Theorem 2 as the multihomogeneous bound for the system minus counts of solutions resulting from Euler's homogeneous function theorem. In particular, the 4-homogeneous Bézout count corresponding with the coefficient of $\alpha_1^{N_1}\alpha_2^{N_2}\beta\zeta^{N_1+N_2}$ in

$$(d_1\alpha_1 + d_2\alpha_2 + \beta)^{N_1+N_2}((d_1-1)\alpha_1 + d_2\alpha_2 + \beta + \zeta)^{N_1}(d_1\alpha_1 + (d_2-1)\alpha_2 + \beta + \zeta)^{N_2}$$

is

$$\binom{N_1+N_2}{N_1}d_1^{N_1-1}d_2^{N_2-1}\left((N_1+N_2+1)(N_1+N_2)d_1d_2 - N_2^2d_1 - N_1^2d_2\right). \quad (12)$$

In this case, one obtains two different types of solutions resulting from Euler's homogeneous function theorem, namely from \mathbb{P}^{N_1} and from \mathbb{P}^{N_2} . The coefficient of $\alpha_1^{N_1-1}\alpha_2^{N_2}\beta$ in $(d_1\alpha_1 + d_2\alpha_2 + \beta)^{N_1+N_2}$ is the count for \mathbb{P}^{N_1} , which is

$$\binom{N_1+N_2}{N_1}N_1d_1^{N_1-1}d_2^{N_2}. \quad (13)$$

Similarly, for \mathbb{P}^{N_2} , the count is

$$\binom{N_1+N_2}{N_1}N_2d_1^{N_1}d_2^{N_2-1}. \quad (14)$$

Thus, subtracting (13) and (14) from (12) yields

$$\binom{N_1 + N_2}{N_1} d_1^{N_1-1} d_2^{N_2-1} ((N_1 + N_2 + 1)(N_1 + N_2)d_1 d_2 - (N_2 + 1)N_2 d_1 - (N_1 + 1)N_1 d_2)$$

which is equivalent to the formula in the statement above. In particular, when $d_1 = d_2 = 1$ and $N_1 = N_2 = N$, this becomes

$$\binom{N + N}{N} ((N + N + 1)(N + N) - (N + 1)N - (N + 1)N) = \binom{2N}{N} (2N^2).$$

□

Example 5. For a bilinear system on $\mathbb{P}^3 \times \mathbb{P}^3$, the bound from Theorem 4 is $2 \cdot 3^2 \cdot \binom{2 \cdot 3}{3} = 360$.

A natural question is to determine the number of branch points for other types of homotopies, such as when the polynomials are defined on multiprojective space and other varieties, with various multidegrees, which is considered in [31]. In particular, results from [31] show that when the polynomials are general, then the exact theoretical predictions on the number of branch points in Theorems 2 and 4 are sharp. However, for particular systems, the exact number of branch points may not be known theoretically. If a few branch points have been missed in these cases, e.g., in Section 5.2, comparison to the general case shows that their number is small enough that it should have little impact on our analysis described in the next section.

4 Impact of branch points

After a choice of γ in (1), the path of $[a, b]$ in (3) when mapped to the Riemann sphere becomes a longitudinal meridian from south pole $(0, 0, -1)$ to north pole $(0, 0, 1)$. Numerical difficulties, or lack thereof, depend on how close this arc passes to a ramification point and on how widespread ill-conditioning is near the branch points. In this section, we present our approach to analyzing these issues given the set of branch points of a homotopy. We also consider what one may expect if the ramification points happen to be distributed uniformly on the Riemann sphere. Subsequently, Section 5 compares the results for specific examples with the expectations for a uniform distribution.

4.1 Distance to ramification points

Assume there are M branch points and an ordering assigned to the branch points and correspondingly to the ramification points. Suppose that the j^{th} ramification point is located at longitude θ_j and latitude ϕ_j . Then, the distance to the meridian of longitude θ is $\delta_j \in [0, \pi/2]$ given by

$$\delta_j(\theta) = \begin{cases} \sin^{-1}(\sin \phi_j \sin |\theta - \theta_j|), & \text{if } |\theta - \theta_j| < \pi/2; \\ \phi_j, & \text{otherwise.} \end{cases} \quad (15)$$

In particular, $\delta_j(\theta)$ is nonnegative and is an even function of $(\theta - \theta_j)$ that is monotonic on intervals $[-\pi, 0]$ and $[0, \pi]$, and zero at $\theta - \theta_j = 0$. Moreover, the function is concave downward or constant everywhere except at its minimum point. For meridians close to the longitude of a ramification point, i.e., for small $(\theta - \theta_j)$, the first-order approximation to (15) is

$$\delta_j(\theta) \approx \sin \phi_j |\theta - \theta_j|, \quad |\theta - \theta_j| \ll 1. \quad (16)$$

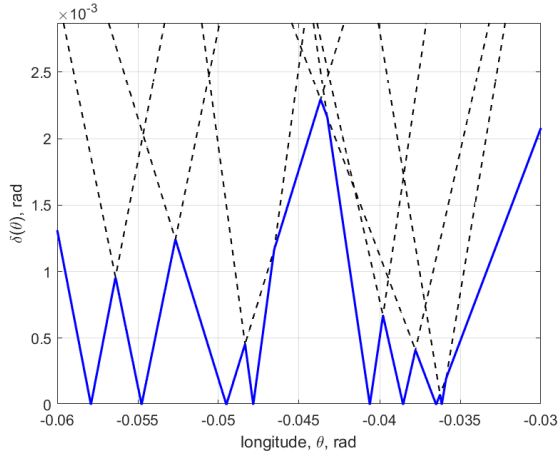


Figure 4: Detail of $\delta_j(\theta)$ and $\delta_{\min}(\theta)$ for $N = 6$ in Example 1. Here, several plots of $\delta_j(\theta)$ are shown as dashed V-shape centered at each longitude θ_j while $\delta_{\min}(\theta)$ is overlaid in solid blue.

Moreover, the periodic function

$$\delta_{\min}(\theta) = \min_{j=1, \dots, M} \delta_j(\theta) \quad (17)$$

touches zero at each $\theta = \theta_j$ and has a single maximum in each interval between adjacent values of θ_j . Figure 4 illustrates this on a small range of longitude. We will be especially interested in the range where (16) applies, which means that we have allocated enough digits of precision to enable solution paths to pass closely by branch points.

4.2 Probability of failure

We wish to investigate how the number of branch points and their distribution affects the probability of success in solving homotopy (1). In practice, this probability depends on many details, such as the scaling of f and g , how their evaluations are coded numerically, and implementation details of the path tracking algorithm. The following definition is a severe simplification of the situation, but it captures the underlying cause of the most common mode of path-tracking failure. Let Z be the set of singular points of homotopy (3), which we partition into $Z = Z_0 \sqcup Z_1 \sqcup Z_B$ as in (4) using the projection $\pi_\tau(u, \tau) \mapsto \tau$.

Definition 6 (δ^* -Failure). Assume that there exists a $\delta^* > 0$ such that path tracking along one-real-dimensional path $\gamma \subset S$, where S is the unit Riemann sphere, succeeds on every solution path if and only if the distance between γ and the nearest singularity satisfies $\delta_{\min}(\theta) \geq \delta^*$. If $\delta_{\min}(\theta) < \delta^*$, the homotopy is said to experience δ^* -failure.

The δ^* -failure criterion is a proxy for failure due to ill-conditioning of the Jacobian matrix h_u . As $[a, b]$ in (3) approaches a branch point, the minimum singular value of h_u approaches 0 on at least one path. This induces a path-tracking failure when progress along the path requires the path tracker to exceed an upper limit set on the number of digits allowed in an adaptive-precision procedure or a lower limit on the forward progress in adaptive step size. Such limits are commonly set as hyperparameters, i.e., a parameter of the path-tracking algorithm, to prevent excessive computation time on particularly difficult paths.

While δ^* -failure ignores some failure modes, it also sets a high bar for success in that we are declaring failure even if only one solution path among many fails.

Theorem 7. Assume $h(u, \tau)$ has no rank deficient solutions at $\tau = [1, 0]$ or $\tau = [0, 1]$. Let $I_{<0}(x)$ be the indicator function that returns 1 if $x < 0$ and 0 otherwise. For θ uniformly distributed over $[-\pi, \pi]$, the probability of δ^* -failure is

$$P_{\text{fail}}(\delta^*) = \frac{1}{2\pi} \int_{-\pi}^{\pi} I_{<0}(\delta_{\min}(\theta) - \delta^*) d\theta. \quad (18)$$

Moreover,

$$\frac{dP_{\text{fail}}}{d\delta^*}(0) = \frac{1}{\pi} \sum_{j=1}^M \frac{1}{\sin \phi_j} \quad (19)$$

Proof. Equation (18) is just expectation of the indicator for failure taken over a uniform distribution. The derivative at zero follows from the first-order approximation (16). \square

Equation (19) indicates that ramification points near the poles, i.e., those with smaller $\sin \phi_j$, are more deleterious than ones in the middle latitudes. That is because a point near a pole is close to a greater proportion of the meridians than a mid-latitude point.

For a given set of branch points, (18) together with (15) and (17) can be used to evaluate P_{fail} . This requires computing the branch points and determining the ramification points where different δ_j enter δ_{\min} . The approximation (19) is much simpler to apply and allows us to consider how δ^* -failure behaves when the ramification points follow a given probability distribution.

Corollary 8. Suppose that M ramification points are distributed independently and uniformly over the Riemann sphere. Then, the expected initial slope of the δ^* -failure curve is $\mathbb{E} \left[\frac{dP_{\text{fail}}}{d\delta^*}(0) \right] = \frac{M}{2}$.

Proof. The latitude ϕ of a point distributed uniformly on the sphere has a probability density function $pdf(\phi) = (\sin \phi)/2$ where $\phi \in [0, \pi]$. Using the initial slope of the failure curve from (19) in Theorem 7, one finds that its expectation is

$$\mathbb{E} \left[\frac{dP_{\text{fail}}}{d\delta^*}(0) \right] = \int_0^\pi \left(\frac{1}{\pi} \sum_{j=1}^M \frac{1}{\sin \phi_j} \frac{\sin \phi_j}{2} \right) d\phi = \frac{M}{2\pi} \int_0^\pi d\phi = \frac{M}{2}.$$

\square

Naturally, a homotopy with more branch points and correspondingly more ramification points will have a higher probability of failure, but it is notable that the rate of increase is only linear in the total number M . Practical experience shows that homotopies with high total degree usually require the allocation of more digits of precision to achieve the same level of robustness as one observes for lower-degree homotopies. One explanatory factor for this observation is that high-degree homotopies tend to have more branch points as suggested by Theorems 2 and 4.

Since the slope given in Corollary 8 is just an expectation, samples of M randomly distributed points can have slopes different from this. Moreover, the actual distribution of ramification points in homotopies may have distributions far from uniform, as observed in Figures 2 and 3.

It should be noted that the variance of the initial slope of P_{fail} is unbounded. This is attributable to the fact that a ramification point close to either pole makes an outsized contribution to the slope, with the contribution tending to infinity the closer it happens to land near a pole. Accordingly, under the assumption of uniform distribution, the average behavior is mild but outliers are expected.

Given a set of branch points and ramification points, we can compute $P_{\text{fail}}(\delta^*)$ from (18) and compare its limiting behavior to the prediction of a uniform distribution. For this purpose, it is

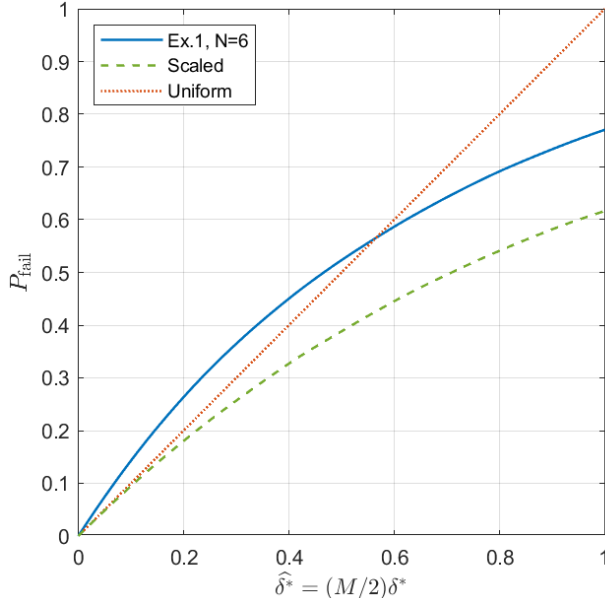


Figure 5: Probability of δ^* -failure, P_{fail} , versus normalized safe distance $\hat{\delta}^*$ for Example 1 and its rescaled counterpart from Section 4.4. The diagonal line shows the slope expected from a uniform distribution of branch points.

useful to plot P_{fail} versus $\hat{\delta}^* = (M/2)\delta^*$ so that the expected slope for the uniform distribution is 1. This normalizes the plot when we consider problems with a different number of branch points. The result for our running example is shown in Figure 5, where we see that the actual distribution of the ramification points gives a steeper slope at the origin than expected from a uniform distribution. The actual slope is approximately 1305 compared to 672 expected for a uniform distribution. This is due to the fact that the ramification points for this example are concentrated in a ring near $z = -1$ as observed in Figure 2. Even though the actual slope is higher than the uniform expectation, we see that they are of approximately the same order of magnitude.

Section 4.5 relates the distance to branch points and conditioning of the Jacobian, which in turn governs how close we may successfully pass by a branch point. For the moment, let us suppose that we have allocated enough digits of precision so that $\delta^* \approx 10^{-6}$, a reasonable number when working in double precision. Under that assumption, we see that the probability of δ^* -failure computed using Theorem 7 on the running example is quite low, only $1.3 \cdot 10^{-3}$. Of course, this can be made even lower by using higher precision.

4.3 Endgame failure

It commonly happens that some of the solution paths of homotopy (3) end at singularities when $f(u)$ has a more special structure than the start system $g(u)$. To compute the endpoint singularities, one may employ a singular endgame, e.g., [18, 23, 24]. For any of these endgames to work reliably, τ must be close enough to $[0, 1]$ to enter the endgame operating zone [24, 32], whose outer radius is governed by the ramification point closest to $[0, 1]$. However, the endgame operating zone also has an inner void due to ill-conditioning near the singularity at $[0, 1]$. If too few digits of precision are used in computations, the inner void may be so large that the endgame operating zone is empty, that is, the endgame will fail.

To be more precise, we will limit our discussion to the “Cauchy endgame” of [23], although the behavior of endgames based on a fractional power series (i.e., Puiseux series) is similar. By the theory described in [23], the topology of curve X in the neighborhood of a singularity in Z_0 is a punctured disk, which can be described as follows. Let $\Gamma(\xi) = [\sin \phi e^{2\pi i \xi}, \cos \phi] \in \mathbb{P}^1$, $\phi < \pi$, $\xi \in [0, 1] \subset \mathbb{R}$, which maps to a circle of constant latitude ϕ on the unit Riemann sphere. Define the interior $\widehat{\Gamma}$ of Γ to be the cap of the sphere that contains $(0, 0, 1)$. Let $P = X \cap \pi_\tau^{-1}(\Gamma(0))$ be a set of points connected by monodromy in X around $\Gamma(\xi)$ and let $\#P$ denote the number of points in P . If $\widehat{\Gamma}$ does not contain a ramification point for X , then continuation in X from P along any path in $\widehat{\Gamma} \setminus \{[0, 1]\}$ is well-defined up to monodromy around $\tau = [0, 1] \in \mathbb{P}^1$, and the set of all such points with the usual topology in \mathbb{C} is topologically equivalent to a punctured disk. Moreover, there is a unique point, say P_0 , that completes the closure of the disk. Each coordinate of P_0 is given by a Cauchy integral circling $\#P$ times around $\Gamma(t)$. The computation of P_0 via such an integral is known as the “Cauchy endgame,” and $\#P$ is called the “winding number” or “cycle number” of the endpoint. Of course, the path of the Cauchy integral does not have to be a circle, but sampling at equal intervals around a circle of constant latitude leads to a simple calculation since the trapezoidal rule for integration nets out to the average of the samples. As explained in [35], this approach has particularly nice computational properties. The endgame applies to both singular and nonsingular endpoints, but it is not usually deployed for nonsingular endpoints since they can be computed by path tracking all the way to $\tau = [0, 1]$.

By the construction above, each singular endpoint of the homotopy has an associated local disk that extends outward until the first branch point is encountered at the outer radius of convergence of the endgame. Call this the singularity’s local branch point (or possibly, branch points) and the corresponding ramification point the singularity’s local ramification point(s). For the endgame to succeed, the path of the Cauchy integral must stay close enough to the singularity to pass between it and the local ramification point(s), but path tracking near the singularity may fail if too few digits of precision are used. The following aims to capture this phenomenon.

Definition 9 (Endgame δ^+ -Failure). For a given working precision near a singular endpoint, there exists a $\delta^+ > 0$ such that path tracking fails for monodromy along a circle of constant latitude $\phi < \delta^+$. We say that the Cauchy endgame executed at latitude $\phi < \delta^+$ for a singular endpoint experiences δ^+ -failure.

Theorem 10. *Suppose that the radius of convergence for a singular endpoint is ϕ^* , and path tracking is subject to δ^* -failure near ramification points and δ^+ failure near the singularity. Then, the Cauchy endgame must fail if $\phi^* < \delta^* + \delta^+$.*

Proof. To succeed, the path of the Cauchy integral must pass between the ramification point at latitude ϕ^* and the singularity at latitude 0, staying δ^* from the former and δ^+ from the latter. If $\phi^* < \delta^* + \delta^+$, these forbidden zones overlap. \square

When $\phi^* > \delta^* + \delta^+$, the Cauchy endgame has an annular endgame operating zone extending from latitude δ^+ to $\phi^* - \delta^*$. When the operating zone is narrow, the Cauchy endgame procedure may have trouble finding a latitude where it succeeds. In practice, the endgame is executed without knowledge of ϕ^* , so success is judged by computing the integral at several different latitudes, for example, at ϕ and at $\alpha\phi$ for $\alpha > 1$ which are both inside the operating zone. A criterion for success is that the convergence rate of the approximation has the expected dependence on ϕ . In such an approach, the procedure needs $\phi^* > \delta^* + \alpha\delta^+$.

The preceding discussion has concentrated on endpoint singularities and the endgame, but in general there could also be singularities at the start of the homotopy. In many applications, this

is not an issue since the start system g is constructed to have all nonsingular roots. However, the start system for polyhedral (a.k.a. BKK) homotopies [17, 36] does begin with singularities, and initiation of path tracking from $\tau = [1, 0]$ depends on the convergence of a fractional power series there. To handle such cases, one may make the obvious adjustments to our discussion here, considering monodromy loops around $[1, 0]$ instead of around $[0, 1]$, and so on.

To analyze the endgame operating zone in detail, one would need to determine the local branch point and corresponding ramification point for each singularity. Lacking this knowledge, we can still say that if all ramification points are farther than $\phi_{\text{crit}} := \delta^* + \delta^+$ from $\tau = [0, 1]$, then the endgame will succeed on every endpoint. To get an idea of how probable this desirable outcome is, we consider the case where the ramification points are uniformly distributed on the sphere.

Proposition 11. *The cumulative distribution function (CDF) and the probability density function (PDF) associated with the minimum latitude of M points distributed independently and uniformly on the unit sphere are*

$$\text{cdf}(\phi_{\min}) = 1 - 2^{-M}(1 + \cos \phi_{\min})^M, \quad \text{pdf}(\phi_{\min}) = \frac{M}{2^M}(1 + \cos \phi)^{M-1} \sin \phi, \quad \phi \in [0, \pi], \quad (20)$$

while the maximum likelihood value (MLE) is

$$\text{mle}(\phi_{\min}) = \arctan 2(\sqrt{2M-1}, M-1) \approx \sqrt{2/M}, \quad M \gg 1. \quad (21)$$

Proof. The z -coordinates of the M points are distributed independently and uniformly on $[-1, 1]$. Latitude $\phi = \cos^{-1} z$ is monotonic on $[-1, 1]$, so the point of minimum ϕ is the point of maximum z . Thus, order statistics, e.g., see [37, § 6.7], followed by a transformation yields (20). Equation (21) derives from setting the derivative of the *pdf* in (20) to zero and solving. \square

Corollary 12. *For large M and small ϕ_{crit} with $M\phi_{\text{crit}}^2 \ll 1$, the probability that the minimum latitude is less than ϕ_{crit} is*

$$P(\phi_{\min} \leq \phi_{\text{crit}}) = \text{cdf}(\phi_{\min}) \approx M\phi_{\text{crit}}^2/4. \quad (22)$$

Proof. This is the first term of a Taylor series for *cdf*(ϕ_{\min}). \square

Theorem 13. *For M points distributed independently and uniformly on the unit sphere, the expected value of the minimum latitude is*

$$E_M := \mathbb{E}[\min(\phi_1, \dots, \phi_M)] = \frac{M}{2^M} \int_{-1}^1 (\xi + 1)^{M-1} \cos^{-1}(\xi) d\xi = M \int_0^1 \xi^{M-1} \cos^{-1}(2\xi - 1) d\xi, \quad (23)$$

which, for large M , is approximately

$$E_M \approx \tilde{E}_M := \frac{M\Gamma(M)\sqrt{\pi}}{\Gamma(M + \frac{3}{2})} \quad (24)$$

$$\approx \sqrt{\pi/M}. \quad (25)$$

Proof. Letting $z_{\max} = \max(z_1, \dots, z_M)$, the first integral above is the expectation of the function $\phi(z_{\max}) = \cos^{-1}(z_{\max})$ using order statistics with z_j uniformly distributed on $[-1, 1]$ [37, § 6.7]. The second integral results from a change of variables arising from mapping $\xi \in [-1, 1]$ to $(2\xi - 1) \in [0, 1]$. For large M , the integrand is negligible except near $\xi = 1$, where we can approximate it as

$$\tilde{E}_M = M \int_0^1 \xi^{M-1} \cdot 2(1 - \xi)^{1/2} d\xi,$$

which leads to (24). Then, (25) follows from $\Gamma(M + 3/2) \approx M^{3/2}\Gamma(M)$. \square

The approximate formulas show that as M grows, the MLE and expected values of ϕ_{\min} approach zero slowly, with the expected value about 25% larger of the two. The slow descent of these values can be understood intuitively by considering that if we draw points at random sequentially, each new minimum establishes a lower probability that any subsequent draw will reduce it further.

The ramification point with the minimum latitude is not necessarily the local ramification point for a singularity, but we may pessimistically assume that it is. When that is so, Theorem 10 says that endgame failure occurs when $\phi_{\min} < \phi_{\text{crit}} = \delta^* + \delta^+$. Under the assumption of uniformly distributed ramification points, (22) shows that we may expect the probability of failure to grow proportional to the number of branch points, but the good news is that lowering ϕ_{crit} by allocating more digits of precision pays off quadratically, as is implied by the condition number analysis given below in Section 4.5.

Example 14 ($2k$ bilinear quadratics with Bézout start system). Let the target system $f(u)$ be a system of $2k$ bilinear, complex quadratics $f(u) = \{f_1, \dots, f_{2k}\}$ of the form

$$f_j = \underline{x}A_j\underline{y}^T, \quad \underline{x} = [1 \quad x_1 \quad \cdots \quad x_k], \quad \underline{y} = [1 \quad y_1 \quad \cdots \quad y_k], \quad u = (\underline{x}, \underline{y}) \in \mathbb{C}^{2k},$$

where each $A_j \in \mathbb{C}^{(k+1) \times (k+1)}$ with elements chosen uniformly within the box $[-1, 1] \times [-i, i] \subset \mathbb{C}$. Since f is a system of quadratics, one option for solving it is via a homotopy where g is a Bézout start system of the form

$$g(u) = \{g_1, \dots, g_{2k}\}, \quad g_j = u_j^2 - 1.$$

The corresponding homotopy (3) has 2^{2k} solutions at $\tau = [1, 0]$ which is the number of solution paths. At $\tau = [0, 1]$, bilinearity causes $V(f)$ to consist of only $\binom{2k}{k}$ nonsingular roots. The difference, namely $2^{2k} - \binom{2k}{k}$, consists of solution paths that diverge to infinity. After homogenizing the homotopy via $\mathbb{C}^{2k} \hookrightarrow \mathbb{P}^{2k}$, we have $h(\underline{u}, \tau) = a\tilde{g}(\underline{u}) + b\tilde{f}(\underline{u})$

$$\begin{aligned} \tilde{f}_j &= \underline{X}A_j\underline{Y}^T, \quad \underline{X} = [u_0 \quad x_1 \quad \cdots \quad x_k], \quad \underline{Y} = [u_0 \quad y_1 \quad \cdots \quad y_k], \\ \underline{u} &= [u_0 \quad x_1 \quad \cdots \quad x_k \quad y_1 \quad \cdots \quad y_k] \in \mathbb{P}^{2k}, \end{aligned}$$

with start system $\tilde{g}_j = u_j^2 - u_0^2$. For computations, we pick a random patch on \mathbb{P}^{2k} , which maps the divergent endpoints in \mathbb{C}^{2k} to finite points in \mathbb{P}^{2k} thus making them easily computable.

With $k = 3$, only $\binom{6}{3} = 20$ of $2^6 = 64$ solution paths end at finite solutions, while the other 44 diverge to infinity as $\tau \rightarrow [0, 1]$. The number of branch points is only 1176 compared to 1344 for a general pencil of 6 quadratics. However, the 44 endpoints at infinity are singular, so a singular endgame is required. A computation of the branch points for a random example gave $\phi_{\min} \approx 0.00118$ which is substantially smaller than the maximum likelihood value of ≈ 0.041 . By (22), the probability of obtaining this minimum value or smaller in 1176 uniformly distributed trials is approximately 4.1×10^{-4} . This implies that a uniform distribution is not a good model for predicting the distribution of ramification points near $\tau = [0, 1]$ for this highly structured homotopy. Assuming that the branch point whose ramification is close to $\tau = [0, 1]$ marks the convergence zone of a singularity, the singular endgame will have to follow a circle of latitude inside that boundary. Enough digits of precision will need to be allocated to track that path as it passes between the ramification point and the singularity at $\tau = [0, 1]$.

Figures 6 and 7 show maps and histograms of the distribution of ramification points for this example. Despite the fact that one ramification point is unexpectedly close to $\tau = [0, 1]$, the general distribution is not skewed in that direction. In fact, most of the ramification points are in the left-hand disk, closer to $\tau = [1, 0]$ than $[0, 1]$.

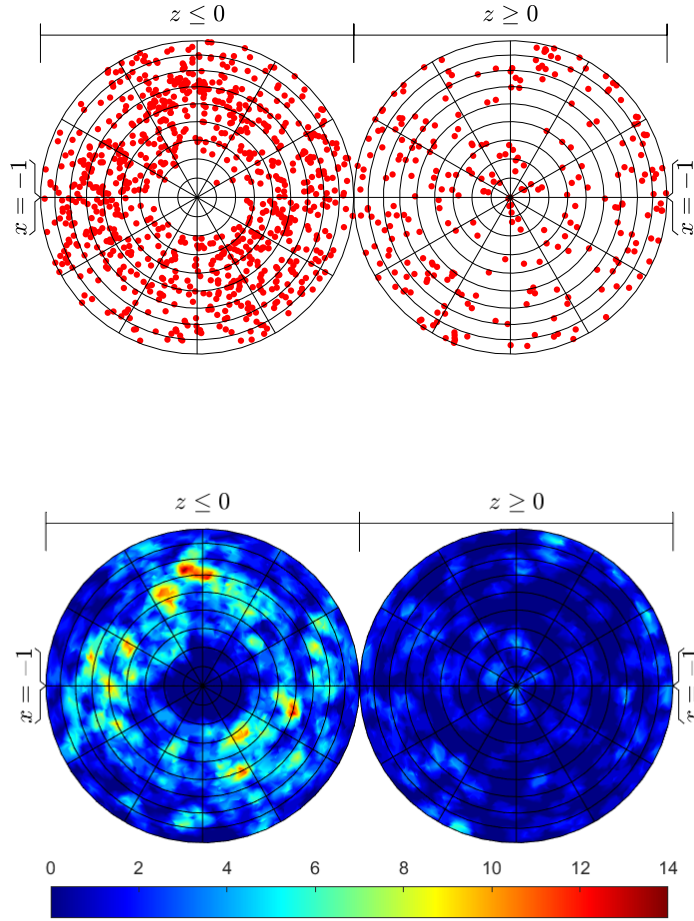


Figure 6: Ramification point scatter plot and heat map for $k = 3$ in Example 14

Figure 8 shows P_{fail} for this same example. The presence of the ramification point near $[0, 1]$ shows up as a sharp jump to $P_{\text{fail}} = 1$ occurring at $\hat{\delta}^* = (M/2)\phi_{\min} \approx 0.69$ for $M = 1176$, $\phi_{\min} = 0.00118$. The initial slope of the failure curve in Figure 8 is 802 compared to an expectation of 588 for a uniform distribution. This higher failure rate is also due to the exceptional ramification point: according to (19), it contributes ≈ 270 to the slope. Note that this implies that the remaining 1175 ramification points actually contribute less than expected for a uniform distribution. This accords with our observation that the bulk of the ramification points are well away from either endpoint of the homotopy path.

4.4 Scaling

We mentioned in the Introduction that previous work has involved scaling, which can help in achieving a high success rate. In the running example, we have seen that the branch points are concentrated in an annulus centered on the start system. The radius of that annulus can be changed simply by scaling the start system. Indeed, changing the pencil to $h(u, [a, b]) = a(6g(u)) + bf(u)$,

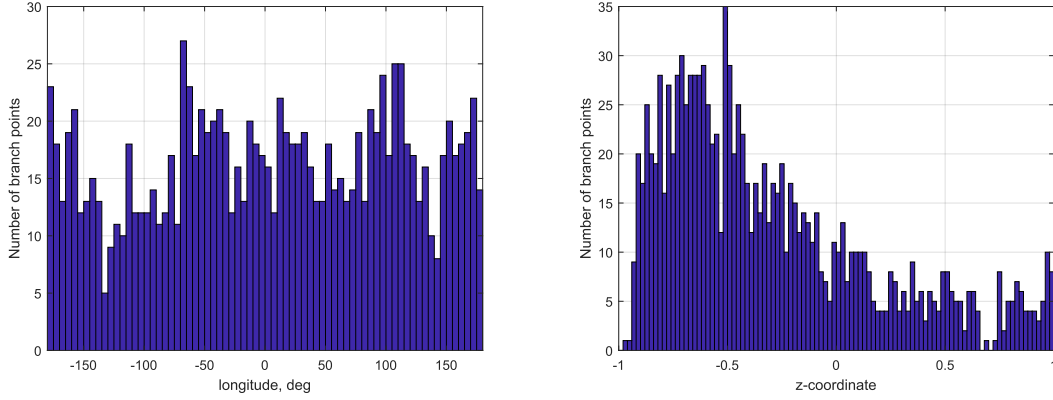


Figure 7: Histogram counts for number of ramification points for Example 14 with $k = 3$ along longitude $[0^\circ, \pm 180^\circ]$ (left) and the z -coordinate $[-1, 1]$ (right).

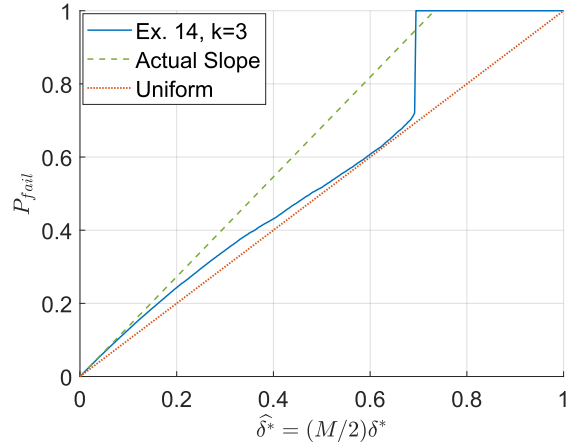


Figure 8: Probability of δ^* -failure, P_{fail} , versus normalized safe distance $\hat{\delta}^*$ for Example 14, $k = 3$. The diagonal red line shows the slope expected from a normal distribution of branch points. The green dotted line is the actual slope of P_{fail} , plotted in blue. The exceptional location of a ramification point close to the pole triggers $\hat{\delta}^*$ -failure at $\hat{\delta}^* \approx 0.69$.

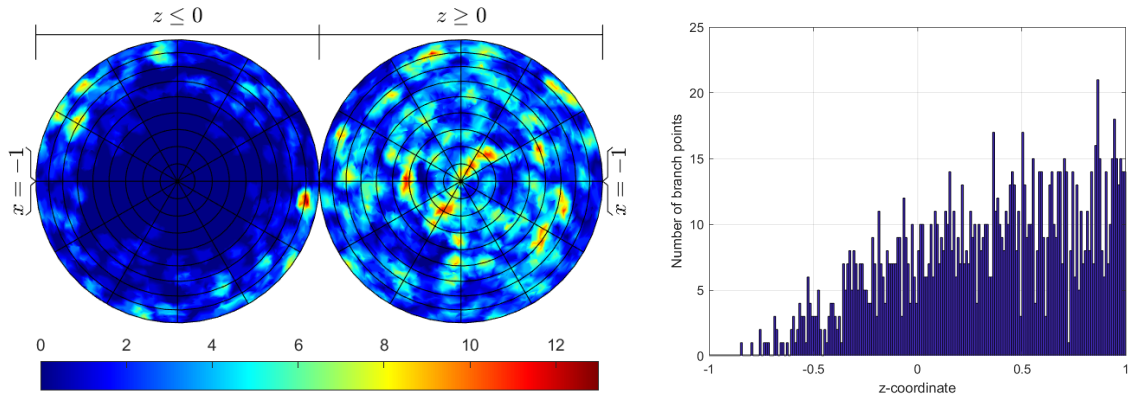


Figure 9: Ramification point density after scaling the start system of Example 1. Compare to Figures 2 and 3, and note change of scale in the color bar and the histogram counts.

where f, g are the same as in Example 1, gives the branch point density shown in Figure 9. This is a more uniform distribution than before scaling; compare it to Figure 2. The upshot is an improved $P_{\text{fail}}(\delta^*)$, as is shown as the dashed curve in Figure 5. In Example 1, the coefficients of f and g are commensurate, but since f is dense with $\binom{N+2}{2}$ terms and g is sparse with just 2 terms in each polynomial, f has a larger scale. The terms in f do not always align, so scaling g by N is sufficient to achieve balance. ($N = 6$ in our running example.)

The practical implication is not so important here since, although we have decreased the failure slope by a factor of 2.6, this is a weaker effect than increasing precision by just one bit, which would decrease δ^* by a factor of 4 (discussed next in Section 4.5). Moreover, whatever improvement scaling makes, it is limited in extent, whereas in principle, precision can be increased indefinitely. However, it does show that if the target system has significantly different scale than the start system, the ramification points will move towards one pole or the other with bad results in either reliability (if precision is fixed) or computation time (if precision is adaptive).

4.5 Condition number near branch points

The argument for using the δ^* -failure criterion is that distance to a branch point strongly correlates with the worst condition number among the solution paths as suggested by Figure 1. Assume that $N \geq 2$ and that (u^*, τ^*) is a branch point of h . For the following analysis, we assume that this branch point arises as a quadratic singularity, which [31] shows is the generic behavior. Hence, $h_u(u^*, \tau^*)$ is rank deficient with $\|h_u(u^*, \tau^*)\| > 0$, i.e., the minimum singular value of $h_u(u^*, \tau^*)$ is zero while the corresponding maximum singular value is nonzero. Moreover, we are assuming that along a solution path $u(\tau) \rightarrow u^*$ as $\tau \rightarrow \tau^*$, one has a first-order approximation of the form

$$\|u(\tau) - u^*\| \sim \|\tau - \tau^*\|^{1/2}, \quad \|\tau - \tau^*\| \ll 1. \quad (26)$$

A Taylor series expansion of $h_u(u(\tau), \tau)$ together with (26) shows that

$$\sigma_{\min}(h_u(u(\tau), \tau)) \lesssim \|\tau - \tau^*\|^{1/2}, \quad \|\tau - \tau^*\| \ll 1. \quad (27)$$

Moreover, $\|h_u(u^*, \tau^*)\| > 0$ yields that

$$\sigma_{\max}(h_u(u(\tau), \tau)) \approx \sigma_{\max}(h_u(u^*, \tau^*)), \quad \|\tau - \tau^*\| \ll 1. \quad (28)$$

Equations (27) and (28) show that the condition number of $h_u(u(\tau), \tau)$ behaves at most similar to $\|\tau - \tau^*\|^{-1/2}$ when $\|\tau - \tau^*\| \ll 1$.

Example 15. To experimentally verify this analysis, we randomly selected a branch point (u^*, τ^*) for the running example with $N = 6$ in Example 1 and randomly selected one of the two paths $(u(\tau), \tau)$ converging to (u^*, τ^*) . Figure 10 plots the relationship between the logarithm of $\|\tau - \tau^*\|$ and the logarithm of the condition number $h_u(u(\tau), \tau)$. Since the slope of this line is approximately $-1/2$, this verifies that the condition number of $h_u(u(\tau), \tau)$ is similar to $\|\tau - \tau^*\|^{-1/2}$.

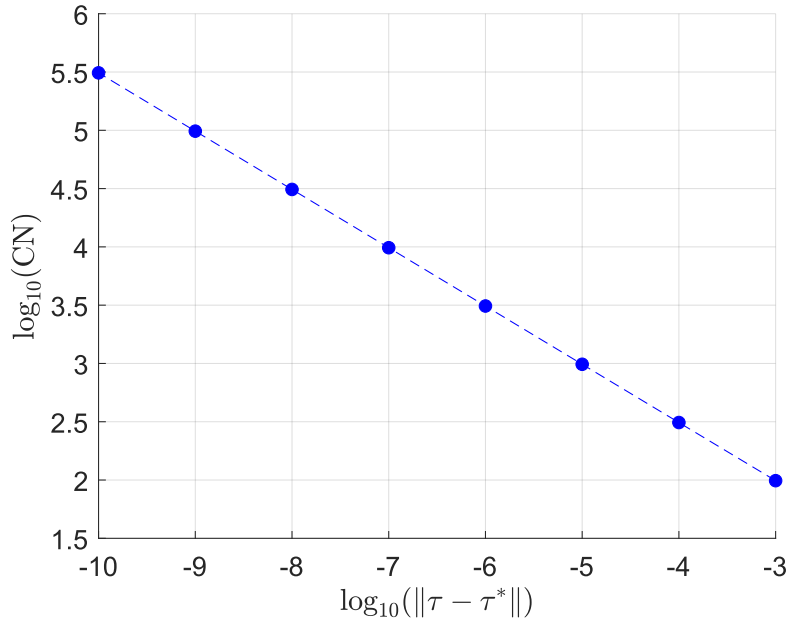


Figure 10: Log-log plot comparing $\|\tau - \tau^*\|$ with the condition number of $h_u(u(\tau), \tau)$ as $\tau \rightarrow \tau^*$ with the slope being approximately $-\frac{1}{2}$.

This analysis is not novel and has been observed in various contexts such as the front cover image of [9], [7, Fig. 2], and [14, Fig. 3.1]. However, the upshot is that, near a branch point, one expects the condition number to behave like the reciprocal of the square root of the distance to the corresponding ramification point. For the current context of successful path tracking, this square root is helping to keep the area of the ill-conditioned regions surrounding the branch points small. In particular, if increasing the working precision by one bit doubles the condition number that one can tolerate, then this square root in the denominator leads roughly to a quartering of the probability of δ^* -failure for each additional bit of precision.

5 Examples

The following considers various quadratic systems (Section 5.1) and a four-bar precision point path synthesis problem (Section 5.2). For these problems, the branch points were computed using Bertini [5, 9]. When the target system has singular solutions, the corresponding bounds on the number of branch points are not sharp. In such cases, the number of branch points reported below is a lower bound on the actual number of branch points in light of the use of numerical computations.

5.1 Quadratic systems

Example 1 considered homotopies in \mathbb{P}^N between the Bézout start system and a target system of N general quadrics, while Example 14 changed the target system to N quadrics bilinear in two groups of $N/2$ variables each. This section considers these cases along with other related systems. In particular, we consider the following six scenarios in \mathbb{P}^N for $N = 6, 8, 10, 12$:

Case	Start system (g)	Target system (f)
1	\mathbb{C} -general quadrics	\mathbb{C} -general quadrics
2	\mathbb{R} -general quadrics	\mathbb{R} -general quadrics
3	Bézout	\mathbb{C} -general quadrics
4	Bézout	\mathbb{R} -general quadrics
5	Bézout	\mathbb{C} -general bilinears
6	Bézout	\mathbb{R} -general bilinears

Here \mathbb{C} -general and \mathbb{R} -general refers to the number field of the coefficients. Coefficients in \mathbb{C} are chosen independently and uniformly in the box $[-1, 1] \times [-i, i]$, while in \mathbb{R} the sample space is the interval $[-1, 1]$. Each start system has 2^N solutions and the first four cases have $\binom{N+1}{2}2^N$ branch points from Theorem 2 which is sharp in light of [31]. The following provides explicit values for $N = 6, 8, 10, 12$:

N	6	8	10	12
2^N	64	256	1024	4096
$\binom{N+1}{2}2^N$	1344	9216	56,320	319,488

Due to the highly structured nature for the last two cases, the number of branch points is expected to be less. The following provides the values computed using `Bertini` for these two cases:

N	6	8	10	12
# branch points	1176	8000	48,840	277,536

The ratio of the number of computed branch points to the generic count $\binom{N+1}{2}2^N$ is about 0.87 for $N = 6, 8, 10, 12$. Hence, there are roughly 13% fewer branch points than the generic case due to the presence of singularities created by targeting a bilinear system inside the family of quadrics.

Let's first consider the distribution of ramification points via histograms of their longitude and latitude. Figure 11 shows histograms of the longitude of the ramification points for the six cases when $N = 12$. In all cases with \mathbb{C} -general coefficients and Case 2 with \mathbb{R} -general coefficients, the longitudes are plausibly distributed uniformly. Cases 4 and 6 with \mathbb{R} -general coefficients show a marked excess of ramification points on the great circle corresponding to the real numbers (longitudes 0° and $\pm 180^\circ$), but are otherwise plausibly uniform.

Figure 12 shows histograms of the z -coordinates of the ramification points. Cases 1 and 2, with general quadrics at the start and target are plausibly distributed uniformly on the Riemann sphere. In all the other cases, the Bézout start system results in a concentrated ring of ramification points near the start system, with a sparse hole immediately surrounding the start system, similar to the illustrations appearing in Section 2.4 for Case 3, $N = 6$. Barely visible in the histograms for Cases 5 and 6 is another ring, albeit smaller, of ramification points around the target system as the deformation from general quadrics to bilinear ones comes to completion.

The second comparison is to consider P_{fail} for the six cases with $N = 6, 8, 10, 12$. In Figure 13, which shows plots of P_{fail} , the abscissa is $\hat{\delta}^* = (M/2)\delta^*$, making the diagonal of the plot box the expected slope at $\delta^* = 0$ (solid line) for a uniform distribution, while the actual slopes are shown as dashed lines. The slopes and their expectations are tabulated in Table 1, where one sees that

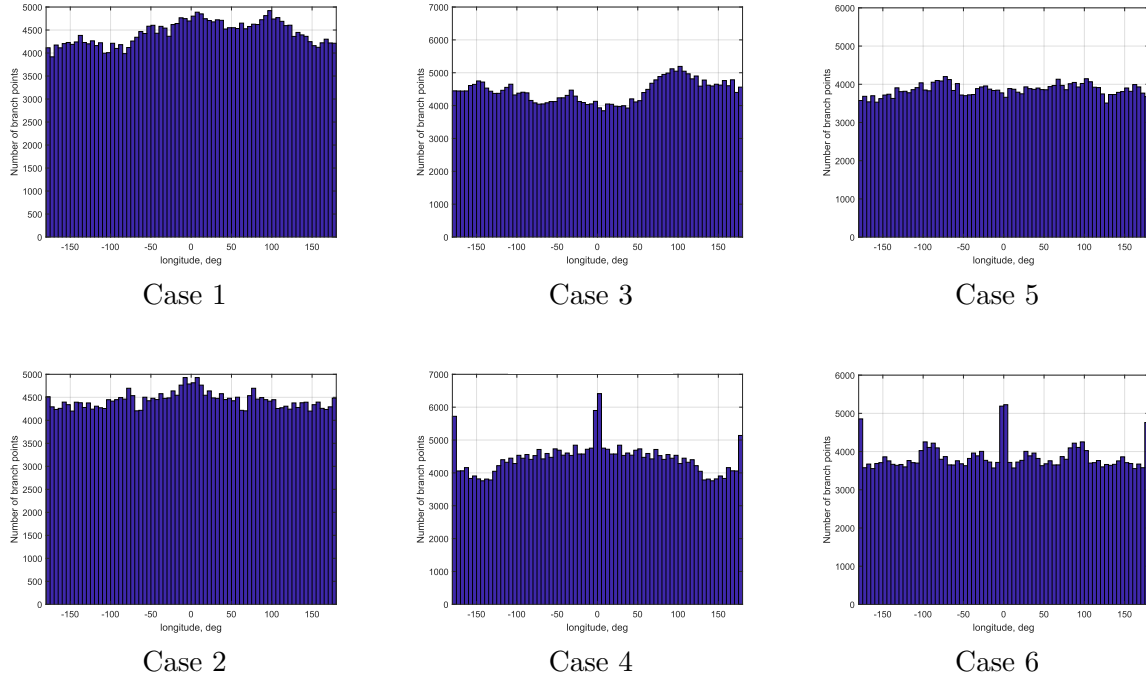


Figure 11: Histograms of the longitude of the ramification points for the six cases with $N = 12$

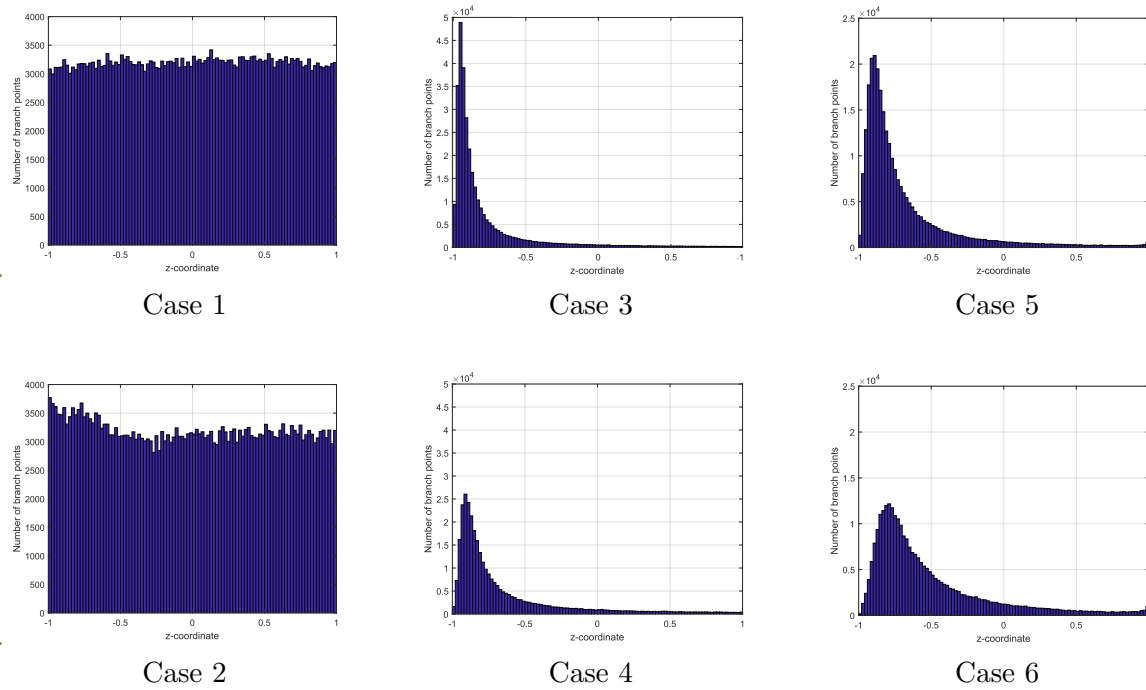


Figure 12: Histograms of the z -coordinates of the ramification points for the six cases with $N = 12$

the actual slope is always of the same order of magnitude as expected. Cases 1 and 2 show the tightest distribution around the expectation, while the largest deviation occurs for Case 3, $N = 12$, where the ratio $S/\mathbb{E}(S) = 1.57$.

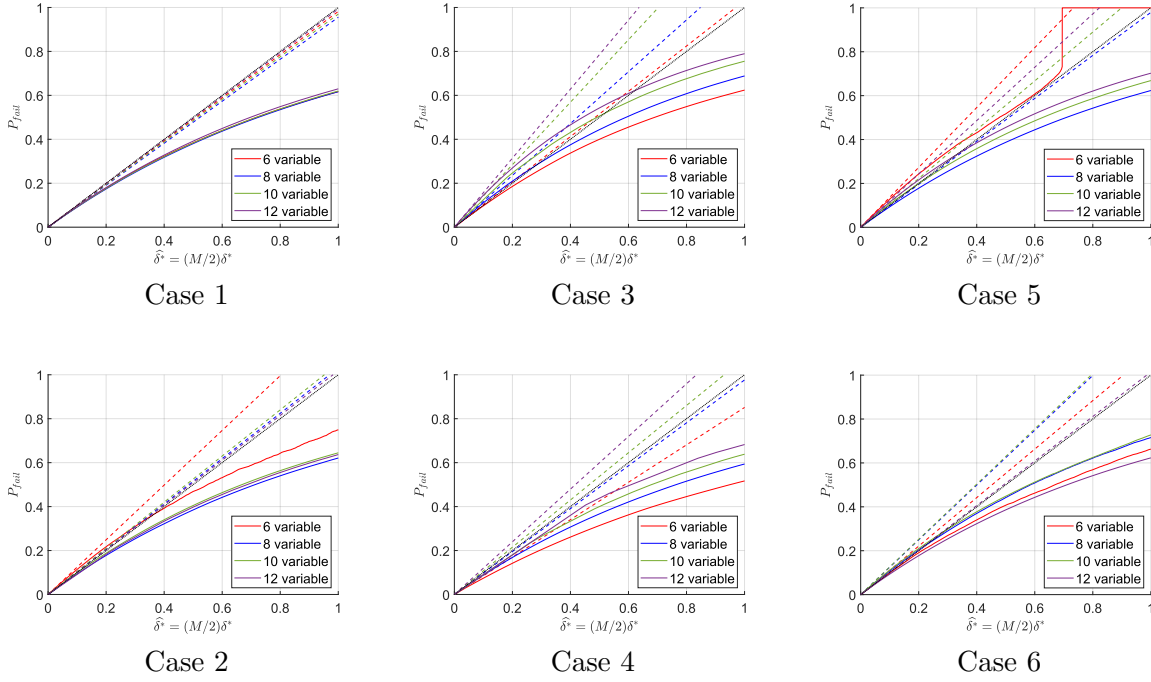


Figure 13: Comparison of P_{fail} for the six cases with $N = 6, 8, 10, 12$

Table 1: Probability of failure slopes, $S = \frac{dP_{\text{fail}}}{d\delta^*}(0)$ for the six cases: expected value, $\mathbb{E}(S)$; actual value, S (rounded off).

Case	$N = 6$		$N = 8$		$N = 10$		$N = 12$	
	$\mathbb{E}(S)$	S	$\mathbb{E}(S)$	S	$\mathbb{E}(S)$	S	$\mathbb{E}(S)$	S
1	672	660.	4608	4403.	28160	27306.	159744	158649.
2	672	836.	4608	4749.	28160	29578.	159744	162689.
3	672	693.	4608	5435.	28160	40045.	159744	250959.
4	672	572.	4608	4499.	28160	30280.	159744	191509.
5	588	802.	4000	3917.	24420	27153.	138768	168656.
6	588	650.	4000	4991.	24420	30744.	138768	140745.

The final comparison is to consider the minimum latitude for the six cases with $N = 6, 8, 10, 12$. Table 2 compares the minimum latitude among the ramification points, ϕ_{\min} , with the expectation from a uniform distribution, E_M , from (24). It also reports $\text{cdf}(\phi_{\min})$ from (20), which is the probability of drawing a sample with that minimum latitude or smaller if the M ramification points were distributed uniformly on the Riemann sphere. Small values of the CDF indicate that it is highly unlikely to have drawn a ϕ_{\min} so small, while values near 1 indicate a that ϕ_{\min} was improbably larger than expected under the assumption of a uniform distribution. Each result is a single sample (we solved one system for each case and size). If one considers probabilities outside of the range $[0.05, 0.95]$ to be significant, one would flag 6 of 24 results as significantly low and 7 of 24 as significantly high. All of the significantly low results occur in Cases 5 and 6. Low values are associated to a greater likelihood of endgame failure, and these are precisely the two cases that have singular endpoints requiring an endgame.

Table 2: Minimum latitude for the six cases: number of branch points, M ; expected minimum latitude, E_M ; actual minimum latitude, ϕ_{\min} ; and $cdf(\phi_{\min})$.

Case	$N = 6$				$N = 8$			
	M	E_M	ϕ_{\min}	cdf	M	E_M	ϕ_{\min}	cdf
1	1344	0.0483	0.0531	0.61	9216	0.0185	0.0285	0.85
2	1344	0.0483	0.0619	0.72	9216	0.0185	0.00580	0.075
3	1344	0.0483	0.0689	0.80	9216	0.0185	0.0672	1.00
4	1344	0.0483	0.168	1.00	9216	0.0185	0.0106	0.23
5	1176	0.0517	0.00118	0.0004	8000	0.0198	0.00968	0.17
6	1176	0.0517	0.00437	0.006	8000	0.0198	0.000367	0.0003

Case	$N = 10$				$N = 12$			
	M	E_M	ϕ_{\min}	cdf	M	E_M	ϕ_{\min}	cdf
1	56320	0.00747	0.0150	0.96	319488	0.00314	0.00136	0.14
2	56320	0.00747	0.00272	0.099	319488	0.00314	0.00462	0.82
3	56320	0.00747	0.0207	1.00	319488	0.00314	0.0349	1.00
4	56320	0.00747	0.0299	1.00	319488	0.00314	0.00916	1.00
5	48840	0.00802	0.0103	0.73	277536	0.00336	0.000725	0.036
6	48840	0.00802	4.7e-5	2.7e-5	277536	0.00336	0.000277	0.0053

5.2 Precision point path synthesis

As mentioned in the Introduction, the nine-point path synthesis problem for four-bar linkages motivated some early experiences with considering branch points of homotopies. Since computing branch points for the nine-point problem is currently beyond the available computational resources, we consider a related problem with fixing one pivot of the four-bar linkage and analyzing the seven-point path synthesis problem illustrated in Figure 14.

Consider following the formulation in [38] using isotropic coordinates in which a real point $(a_x, a_y) \in \mathbb{R}^2$ is mapped to the complex vector $(a, \bar{a}) = (a_x + a_y i, a_x - a_y i) \in \mathbb{C}^2$. The two pivot locations are $A = (a, \bar{a})$, which is assumed fixed, and $B = (b, \bar{b})$. Two sides of the coupler triangle are given by $X = (x, \bar{x})$ and $Y = (y, \bar{y})$. To reduce the total degree of the system, auxiliary variables (n, \bar{n}) and (m, \bar{m}) are introduced along with four conditions:

$$n - a\bar{x} = \bar{n} - \bar{a}x = m - b\bar{y} = \bar{m} - \bar{b}y = 0 \quad (29)$$

We translate the coordinate system to place its origin at the first precision point, $D_0 = (0, 0)$, and we construct the four-bar with its coupler point at the origin as well. This satisfies the requirement to interpolate D_0 . Thus, the coupler curve passes through each of the other six points, say $(d, \bar{d}) \in \{D_1, \dots, D_6\}$, provided that

$$C_{(d, \bar{d})} = \rho_{(d, \bar{d})} \bar{\rho}_{(d, \bar{d})} + \rho_{(d, \bar{d})} \rho_{(d, \bar{d})}^0 + \bar{\rho}_{(d, \bar{d})} \rho_{(d, \bar{d})}^0 = 0 \quad (30)$$

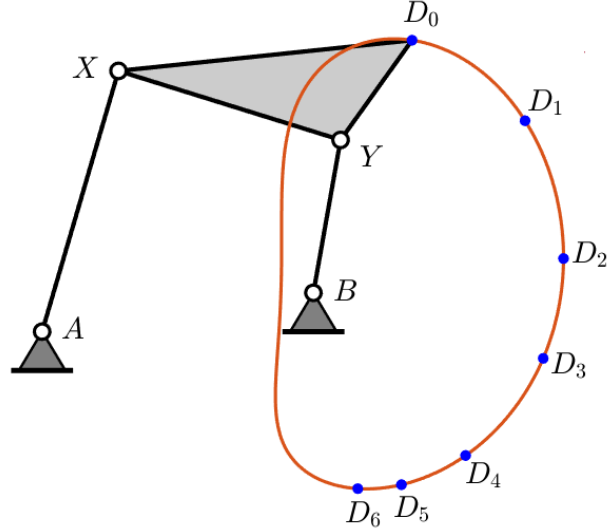


Figure 14: The seven-point path synthesis problem is to find all four-bars (one of which is drawn) whose coupler point passes through the precision points D_0, \dots, D_6 . Ground pivot A is given, but pivot B and the lengths of the five segments composing the mechanism are variables to be found.

where

$$\begin{aligned} \rho_{(d,\bar{d})} &= \det \begin{bmatrix} n - d\bar{x} & d(\bar{a} - \bar{x}) + \bar{d}(a - x) - d\bar{d} \\ m - d\bar{y} & d(\bar{b} - \bar{y}) + \bar{d}(b - y) - d\bar{d} \end{bmatrix}, \\ \bar{\rho}_{(d,\bar{d})} &= \det \begin{bmatrix} d(\bar{a} - \bar{x}) + \bar{d}(a - x) - d\bar{d} & \bar{n} - \bar{d}x \\ d(\bar{b} - \bar{y}) + \bar{d}(b - y) - d\bar{d} & \bar{m} - \bar{d}y \end{bmatrix}, \text{ and} \\ \rho_{(d,\bar{d})}^0 &= \det \begin{bmatrix} \bar{n} - \bar{d}x & n - d\bar{x} \\ \bar{m} - \bar{d}y & m - d\bar{y} \end{bmatrix}. \end{aligned}$$

When pivot $A = (a, \bar{a})$ is fixed the polynomial system for the 7-point path synthesis problem, with precision points $D_j = (d_j, \bar{d}_j)$, $j = 1, \dots, 6$, becomes

$$f(x, \bar{x}, n, \bar{n}, b, \bar{b}, y, \bar{y}, m, \bar{m}) = \left\{ n - a\bar{x}, \bar{n} - \bar{a}x, m - b\bar{y}, \bar{m} - \bar{b}y, (C_{(d_j, \bar{d}_j)}, j = 1, \dots, 6) \right\}. \quad (31)$$

In \mathbb{C}^{10} , f consists of two linear, two quadratic, and six quartic polynomials yielding a Bézout bound of 16,384. Using [31], the generic number of branch points is 1,564,672. Rather than work in \mathbb{C}^{10} , we utilize the natural 2-homogeneous structure among the variables is given by $\{x, \bar{x}, n, \bar{n}\}$ and $\{b, \bar{b}, y, \bar{y}, m, \bar{m}\}$. Hence, (31) consists of two polynomials of bidegree $(1, 0)$, two polynomials of bidegree $(0, 2)$, and six polynomials of bidegree $(2, 2)$ with 2-homogeneous Bézout bound of 3840. Using [31], the generic number of branch points using a homotopy with this bidegree structure is 351,744. For generic data, $f = 0$ has 486 isolated solutions, which arise in cognate pairs, and mechanically-degenerate positive-dimensional components. Due to the positive-dimensional components, the generic number of branch points is expected to be smaller than 351,744.

Consider using two different start systems with the same bidegree structure. First, we used a start system constructed with the first four polynomials being $n - 1, \bar{n} - 1, m^2 - 1, \bar{m}^2 - 1$ and the remaining 6 polynomials being linear products of bidegree $(2, 2)$ with dense linears in $\{x, \hat{x}\}$ and $\{b, \hat{b}, y, \hat{y}\}$, and general coefficients. Second, we used a dense start system with the same bidegree structure having general coefficients. In both start systems, all coefficients were chosen

independently and uniformly on the unit circle in the complex plane, i.e., $z \cdot \text{conj}(z) = 1$. Afterward, to establish scale, both f and g were evaluated at a point with each variable chosen at random on the complex unit circle. Then, g was re-scaled to cg using single constant, $c = \|f\|/\|g\|$.

Our computations found 305,806 branch points for the linear product start system and 313,760 branch points for the dense start system. As suggested in the Section 3, these may not be the exact number of branch points, but since we expect fewer than the upper bound of 351,744, it is reasonable to believe that not many were missed. As long as none were missed extremely close to the start or end, the following analysis and illustrations would not change substantially.

For homotopies using the two start systems, Figure 15 shows P_{fail} , longitude, and z -coordinate while Figure 16 shows the ramification point density using a smoothing radius of 0.08rad. A comparison of these plots shows two different behaviors on the distribution of ramification points. When using a linear product, high density regions of ramification points were clustered around both the start and target systems as well as the point corresponding to infinity. These give a slope of the P_{fail} curve approximately $31(M/2)$. When using a dense multihomogeneous start system, the ramification points were more uniformly distributed with a high density region only near the target system. Eliminating branch points near the start would seem to give the dense system an advantage, but a few points very near the end ruin this, giving a slope of approximately $65(M/2)$ for the P_{fail} curve. For points distributed uniformly on the Riemann sphere, the expected minimum latitude in both cases is $E_M \approx 3.2 \cdot 10^{-3}$, while the actual minima were $1.9 \cdot 10^{-6}$ and $4.4 \cdot 10^{-8}$. These ramification points close to the end of the homotopy path have an outsize influence on the failure slope. In the case of the dense start system, the one extremely close point contributes $46(M/2)$ of the total slope of $65(M/2)$.

Although the linear product start system shows a minor advantage in the failure slope, its main advantage over using a dense system is the ease of computing the start points.

6 Conclusion and discussion

We have considered the number and distribution of branch points for homotopies for solving systems of polynomial equations. After mapping the associated ramification points to the Riemann sphere, we look at how the distribution of these points impact the success of path tracking where “success” means that *every* path is tracked successfully to completion. We present several ways of visualizing the distribution of the ramification points and show how the impact can be summarized as a failure curve $P_{\text{fail}}(\delta^*)$, defined as the probability that a randomly selected homotopy path will pass within a distance of δ^* to a ramification point, measured on the Riemann sphere. The slope as $\delta^* \rightarrow 0$ is of special interest, as this directly relates to how much floating-point precision must be allocated to achieve a desired success rate. Furthermore, if the target system has singular endpoints, then the success or failure of the singular endgame, here assumed to be based on a Cauchy integral, depends on the location of the branch points of the paths leading to singularities. The endgame requires tracking paths around a monodromy loop that must pass between the end of the homotopy path and the nearest ramification point. If this gap is narrow, numerical ill-conditioning must be expected.

One should understand that numerical difficulties are due to ill-conditioning of the solution paths which arise from the inverse image of the homotopy path on the Riemann sphere. In general, each ramification point represents the crossing of just two solution paths at the associated branch point (see [31]). Perturbing the homotopy path from one that passes through a ramification point results in two solution paths passing near the branch point. These two paths will be the ones encountering the greatest numerical difficulties for the perturbed homotopy path. If one uses an adaptive precision algorithm, high precision can be invoked only as necessary. In some applications,

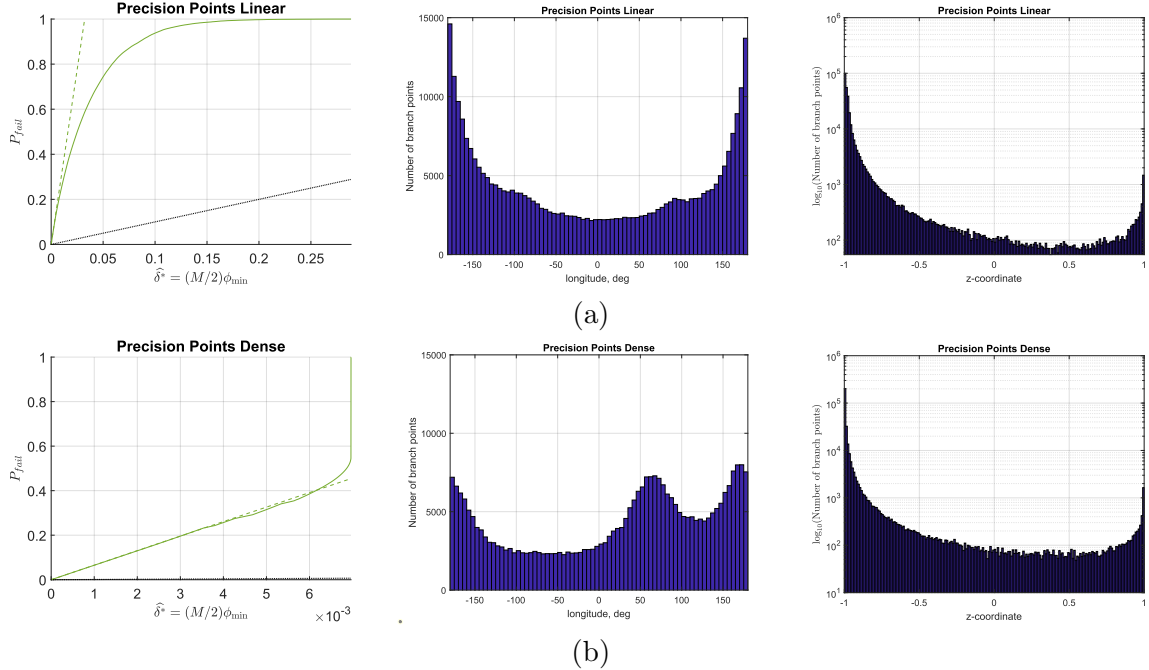


Figure 15: Comparison of solving 7-point problem with one fixed pivot using (a) linear product start system and (b) dense start system. The scaling pushes ramification points towards the start system, resulting in a highly skewed z -coordinate histogram. To visualize this, the histogram plot of the z -coordinate on the right uses a logarithmic (\log_{10}) vertical axis.

such as the path synthesis problem, one may elect to save computation by simply discarding a few problematic solution paths; endpoints that are singular or near singular are often useless as a solution to an engineering problem. In contrast, our definition of success in this article assumes that a complete solution list is paramount.

The actual distribution of branch points is studied on examples where the start and target systems are systems of quadrics and an example from kinematics concerning four-bar path synthesis. We find that when the start and target systems are general quadrics with coefficients in \mathbb{C} , the ramification points appear to be uniformly distributed on the Riemann sphere. This largely remains true also for coefficients in \mathbb{R} , except for the presence of real ramification points appearing on the corresponding great circle on the sphere. Systems of quadrics with a Bézout start system, by which we mean one with polynomials of the form $g_j = z_j^2 - z_0^2$ for $j = 1, \dots, N$, have a notable departure from uniform distribution: although the longitude of the ramification points seems to be distributed uniformly, the same does not appear to hold for latitude. In particular, there appears to be an empty disk centered on the start system with a ring of concentrated ramification points around its perimeter. Such analysis on the distribution of ramification points is particularly important when using monodromy to compute solutions of polynomial systems.

Despite departures from having a uniform distribution, the net effect on the initial failure slope, $\frac{dP_{\text{fail}}}{d\delta^*}(0)$, is minimal. The expected slope for a uniform distribution is $M/2$ (Theorem 8), where M is the number of branch points. For the systems of quadrics, the largest deviation from this expectation was $1.57(M/2)$, while for the path synthesis example it was a more substantial departure of $65(M/2)$. Based on these examples, we posit that $M/2$ is a good rule of thumb for the failure slope that should apply more generally. Establishing this more firmly, either by further experiments or preferably through a suitably developed theory, is an interesting question for further

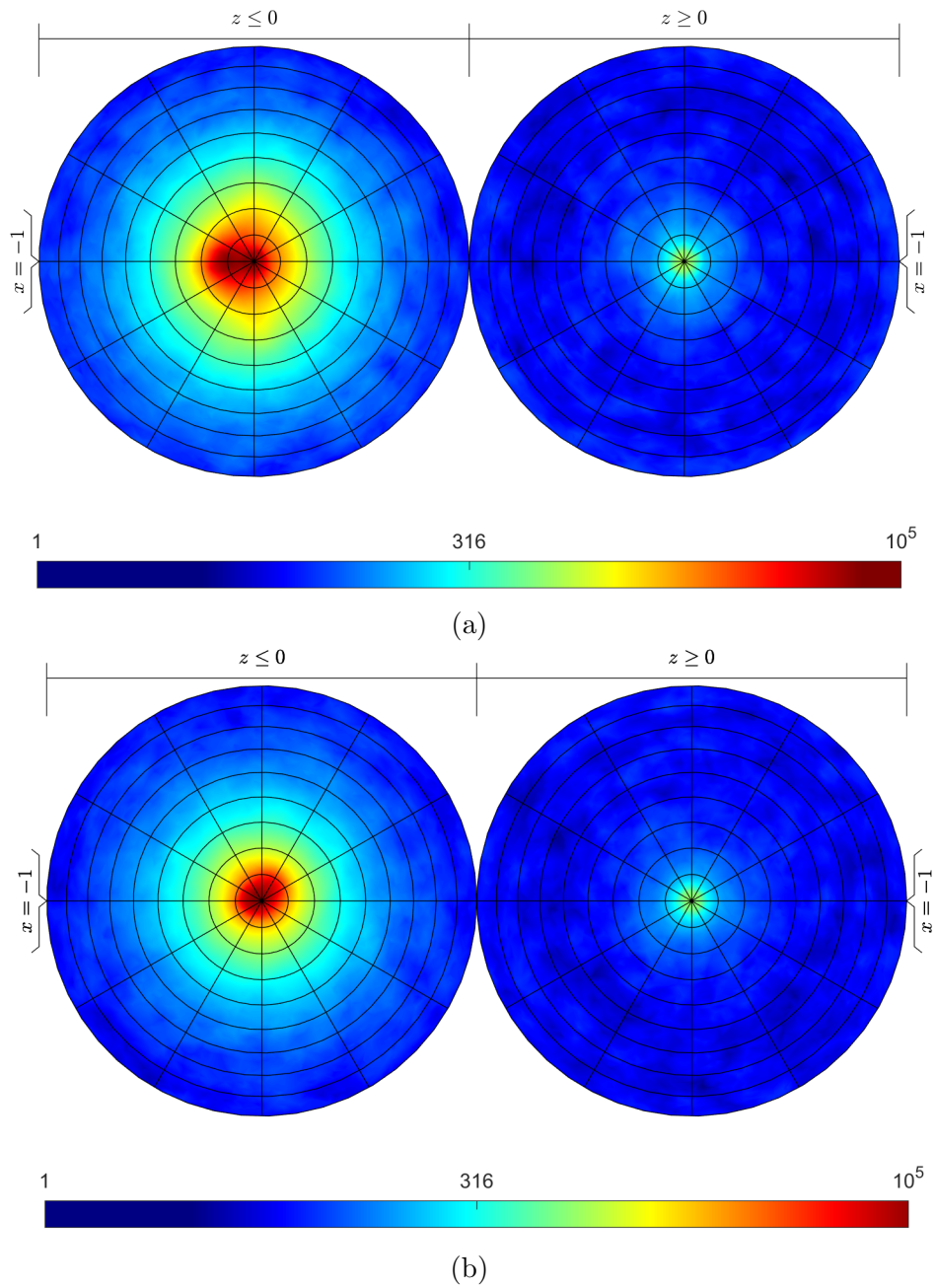


Figure 16: Ramification point density for solving 7-point problem with one fixed pivot using (a) linear product start system and (b) dense start system.

study. The slope is heavily influenced by the ramification points closest to the start or end of the homotopy path, and the largest departures from $M/2$ were for systems whose homotopies had singular endpoints due to the special structures of their target systems. If this is indeed a general phenomenon, then understanding how singular endpoints induce nearby branch points might lead to the construction of more reliable homotopies.

The distribution of the latitude of ramification points is directly affected by the relative scaling of the start and target systems, as illustrated by the example treated in Section 4.4. Re-scaling the start system from g to αg for $|\alpha| > 1$ automatically pushes the ramification points towards the end while $|\alpha| < 1$ pulls them to the start. Bad scaling in either direction will result in a system that requires the use of higher precision than would otherwise suffice.

Theorem 2 provided an upper bound on the number of branch points when all polynomials are general of the same degree and Theorem 4 refined this for the case where all polynomials defined on a product of two projective spaces are general and have the same bidegree. An enumeration of branch points for more types of homotopies, e.g., homotopies where the polynomials have different degrees and are defined on products of several projective spaces, is considered in [31].

References

- [1] E. L. Allgower and K. Georg. *Introduction to Numerical Continuation Methods*. Society for Industrial and Applied Mathematics, 2003.
- [2] D. Armentano. Complexity of path-following methods for the eigenvalue problem. *Found. Comput. Math.*, 14(2):185–236, 2014.
- [3] D. J. Bates, J. D. Hauenstein, C. Peterson, and A. J. Sommese. *Numerical Decomposition of the Rank-Deficiency Set of a Matrix of Multivariate Polynomials*, pages 55–77. Springer, Vienna, 2010.
- [4] D. J. Bates, J. D. Hauenstein, and A. J. Sommese. Efficient path tracking methods. *Num. Algorithms*, 58(4):451–459, 2011.
- [5] D. J. Bates, J. D. Hauenstein, A. J. Sommese, and C. W. Wampler. Bertini: Software for numerical algebraic geometry. Available at bertini.nd.edu with permanent doi: [dx.doi.org/10.7274/R0H41PB5](https://doi.org/10.7274/R0H41PB5).
- [6] D. J. Bates, J. D. Hauenstein, A. J. Sommese, and C. W. Wampler. Adaptive multiprecision path tracking. *SIAM Journal on Numerical Analysis*, 46(2):722–746, 2008.
- [7] D. J. Bates, J. D. Hauenstein, A. J. Sommese, and C. Wampler II. Stepsize control for path tracking. *Contemporary Mathematics*, 496:21, 2009.
- [8] D. J. Bates and M. Niemerg. Using monodromy to avoid high precision in homotopy continuation. *Mathematics in Computer Science*, 8(2):253–262, Jun 2014.
- [9] D. J. Bates, A. J. Sommese, J. D. Hauenstein, and C. W. Wampler. *Numerically solving polynomial systems with Bertini*. SIAM, 2013.
- [10] C. Beltrán and A. Leykin. Robust certified numerical homotopy tracking. *Foundations of Computational Mathematics*, 13:253–295, 2013.

- [11] C. Beltrán and M. Shub. Complexity of Bezout’s theorem. VII. Distance estimates in the condition metric. *Found. Comput. Math.*, 9(2):179–195, 2009.
- [12] P. Bürgisser and F. Cucker. *Condition: The Geometry of Numerical Algorithms*, volume 349 of *Grundlehren der mathematischen Wissenschaften [Fundamental Principles of Mathematical Sciences]*. Springer, Heidelberg, 2013.
- [13] T. Chen and T.-Y. Li. Spherical projective path tracking for homotopy continuation methods. *Communication in Information and Systems*, 12(3):195–220, 2012.
- [14] W. Hao, J. D. Hauenstein, B. Hu, Y. Liu, A. J. Sommese, and Y.-T. Zhang. Continuation along bifurcation branches for a tumor model with a necrotic core. *J. Sci. Comput.*, 53:395–413, 2012.
- [15] J. D. Hauenstein and A. C. Liddell, Jr. Certified predictor-corrector tracking for newton homotopies. *J. Symb. Comput.*, 74:239–254, 2016.
- [16] J. D. Hauenstein and M. H. Regan. Adaptive strategies for solving parameterized systems using homotopy continuation. *Applied Mathematics and Computation*, 332:19–34, 2018.
- [17] B. Huber and B. Sturmfels. A polyhedral method for solving sparse polynomial systems. *Mathematics of computation*, 64(212):1541–1555, 1995.
- [18] B. Huber and J. Verschelde. Polyhedral end games for polynomial continuation. *Numerical Algorithms*, 18:91–108, 1998.
- [19] R. B. Kearfott and Z. Xing. An interval step control for continuation methods. *SIAM Journal on Numerical Analysis*, 31(3):892–914, 1994.
- [20] A. P. Morgan. A transformation to avoid solutions at infinity for polynomial systems. *Appl. Math. Comput.*, 18(1):77–86, 1986.
- [21] A. P. Morgan. *Solving Polynomial Systems Using Continuation for Engineering and Scientific Problems*. Society for Industrial and Applied Mathematics, 2009.
- [22] A. P. Morgan and A. J. Sommese. Coefficient-parameter polynomial continuation. *Appl. Math. Comput.*, 29(2):123–160, 1989. Errata: *Appl. Math. Comput.* 51:207 (1992).
- [23] A. P. Morgan, A. J. Sommese, and C. W. Wampler. Computing singular solutions to nonlinear analytic systems. *Numerische Mathematik*, 58:669–684, 1991.
- [24] A. P. Morgan, A. J. Sommese, and C. W. Wampler. A power series method for computing singular solutions to nonlinear analytic systems. *Numerische Mathematik*, 63:391–409, 1992.
- [25] M. Shub. Complexity of Bezout’s theorem. VI. Geodesics in the condition (number) metric. *Found. Comput. Math.*, 9(2):171–178, 2009.
- [26] M. Shub and S. Smale. Complexity of Bézout’s theorem. I. Geometric aspects. *J. Amer. Math. Soc.*, 6(2):459–501, 1993.
- [27] M. Shub and S. Smale. Complexity of Bezout’s theorem. II. Volumes and probabilities. In *Computational algebraic geometry (Nice, 1992)*, volume 109 of *Progr. Math.*, pages 267–285. Birkhäuser Boston, Boston, MA, 1993.

- [28] M. Shub and S. Smale. Complexity of Bezout’s theorem. III. Condition number and packing. *J. Complexity*, 9(1):4–14, 1993.
- [29] M. Shub and S. Smale. Complexity of Bezout’s theorem. V. Polynomial time. *Theoret. Comput. Sci.*, 133(1):141–164, 1994.
- [30] M. Shub and S. Smale. Complexity of Bezout’s theorem. IV. Probability of success; extensions. *SIAM J. Numer. Anal.*, 33(1):128–148, 1996.
- [31] A. J. Sommese, J. D. Hauenstein, C. Hills, and C. W. Wampler. Branch points of homotopies: Enumeration and general theory. submitted.
- [32] A. J. Sommese and C. W. Wampler. *The Numerical Solution of Systems of Polynomials Arising in Engineering and Science*. World Scientific Publishing Co. Pte. Ltd., Hackensack, NJ, 2005.
- [33] S. Telen, M. V. Barel, and J. Verschelde. A robust numerical path tracking algorithm for polynomial homotopy continuation. *SIAM Journal on Scientific Computing*, 42(6):A3610–A3637, 2020.
- [34] S. Timme. Mixed precision path tracking for polynomial homotopy continuation. *Advances in Computational Mathematics*, 47(5):75, 2021.
- [35] L. N. Trefethen and J. Weideman. The exponentially convergent trapezoidal rule. *SIAM review*, 56(3):385–458, 2014.
- [36] J. Verschelde, P. Verlinden, and R. Cools. Homotopies exploiting newton polytopes for solving sparse polynomial systems. *SIAM Journal on Numerical Analysis*, 31(3):915–930, 1994.
- [37] D. D. Wackerly, W. Mendenhall III, and R. L. Scheaffer. *Mathematical Statistics with Applications*. Thomson Brooks/Cole, Belmont, CA, seventh edition, 2008.
- [38] C. W. Wampler, A. P. Morgan, and A. J. Sommese. Complete solution of the nine-point path synthesis problem for four-bar linkages. *J. Mech. Design*, 114:153–159, 1992.